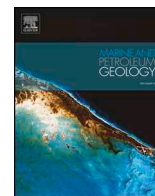




ELSEVIER

Contents lists available at ScienceDirect

## Marine and Petroleum Geology

journal homepage: [www.elsevier.com/locate/marpetgeo](http://www.elsevier.com/locate/marpetgeo)

Research paper

# Kinematic and mechanic evolution of the Andes buried front at the Boomerang Hills hydrocarbon province (Bolivia): Control exerted by the pre-Andean history

Hodei Uzkeda<sup>a,\*</sup>, Mayte Bulnes<sup>a</sup>, Josep Poblet<sup>a</sup>, Gonzalo Zamora<sup>b</sup><sup>a</sup> Departamento de Geología, Universidad de Oviedo, C/Jesús Arias de Velasco s/n, Oviedo, 33005, Spain<sup>b</sup> Repsol Exploración S.A., C/Méndez Álvaro 44, Madrid, 28045, Spain

## ARTICLE INFO

## Keywords:

3D geological model  
Andes  
Boomerang hills  
Inversion tectonics  
Sequential restoration

## ABSTRACT

The Boomerang Hills are a hydrocarbon-rich region located in front of the Bolivian Andes, central South America, where the Andean chain bends forming the Bolivian Orocline. The geological interpretation of seismic (2D profiles and 3D volumes) and well data allowed us to generate a complete stratigraphic section, cross sections, maps and a 3D model, and to obtain the parameters to carry out a depth conversion and decompaction. A cross section and a 3D model were kinematically and mechanically restored, as well as decompacted, to decipher the evolution of this region through time. The southern Boomerang Hills are the buried frontal part of the Andes where thin-skinned contractional structures of Andean age (Late Cenozoic) predominate, whereas the northern Boomerang Hills belong to the Beni-Chaco Plain, where contractional structures are almost absent and thick-skinned extensional tectonics of pre-Andean age (Paleozoic, Mesozoic and Early Cenozoic) dominate. The buried frontal thrust of the Andes resulted from transpressional reactivation of a gravity-driven, extensional detachment developed along the slope of a basement high tilted during Paleozoic times. Thus, the thrust orientation, position, dimensions and type of structural termination were controlled by the extensional fault geometry, the Paleozoic mechanical stratigraphy, and the structural relationships between the Paleozoic cover and the basement.

## 1. Introduction

The Boomerang Hills constitutes one of the main prospective areas in terms of hydrocarbons in central Bolivia (Fig. 1) and has been extensively explored from the sixties. Several 2D and 3D seismic surveys have been acquired and hundreds of wells have been drilled in this area, and more than 250 have tested hydrocarbons. Unraveling the geology of the Boomerang Hills using surface data is unsatisfactory because only the upper part of the Cenozoic succession crops out, thus the good seismic and well coverage provides an excellent dataset to do so. In addition to its economic interest, this region is remarkable from a structural point of view because of two reasons: 1) a combination of extensional, contractional and inversion tectonics structures, due to different tectonic events, configure this area; and 2) the general trend of the Andean Cordillera bends from NW-SE to the northwest, to WNW-ESE near the Boomerang Hills, to N-S to the southeast (Fig. 1) as part of the so-called Bolivian Orocline (e.g. Carey, 1958; Isacks, 1988). The most significant stratigraphic feature of the Boomerang Hills is a

pervasive angular unconformity at the base of the Mesozoic sequence that truncates progressively older Paleozoic rocks towards the north.

Although some geological issues have been addressed in previous publications such as Baby et al. (1994, 1995), Welsink et al. (1995a), Laffite et al. (1998), Kley (1999), Giraudo and Limachi (2001), Hinsch et al. (2002, 2003), Husson and Moretti (2002), there are still important aspects to understand regarding the stratigraphy and structure of the Boomerang Hills as, for instance, the control exerted by previous structures and stratigraphy on the Andean deformation. Baby et al. (1995) analyzed the source rocks and carried out petroleum modeling in order to decipher when they entered the hydrocarbon generation window. Welsink et al. (1995a) described the geology using seismic lines and well data, and defined two structural domains based on the most common structures and the stratigraphic sequence. Laffite et al. (1998) analyzed the main hydrocarbon parameters, such as maturation, TOC (Total Organic Carbon), TAI (Thermal Alteration Index) and Ro (vitrinite reflectance) values. Kley (1999) constructed a kinematic model of the Bolivian Orocline (from Peru to Chile) using restored sections and

\* Corresponding author.

E-mail addresses: [hodei@geol.uniovi.es](mailto:hodei@geol.uniovi.es) (H. Uzkeda), [maite@geol.uniovi.es](mailto:maite@geol.uniovi.es) (M. Bulnes), [jpoblet@geol.uniovi.es](mailto:jpoblet@geol.uniovi.es) (J. Poblet), [gzamorav@repsol.com](mailto:gzamorav@repsol.com) (G. Zamora).<https://doi.org/10.1016/j.marpetgeo.2020.104299>

Received 4 October 2019; Received in revised form 11 February 2020; Accepted 13 February 2020

Available online 19 February 2020

0264-8172/ © 2020 The Authors. Published by Elsevier Ltd. This is an open access article under the CC BY-NC-ND license

<http://creativecommons.org/licenses/by-nc-nd/4.0/>.

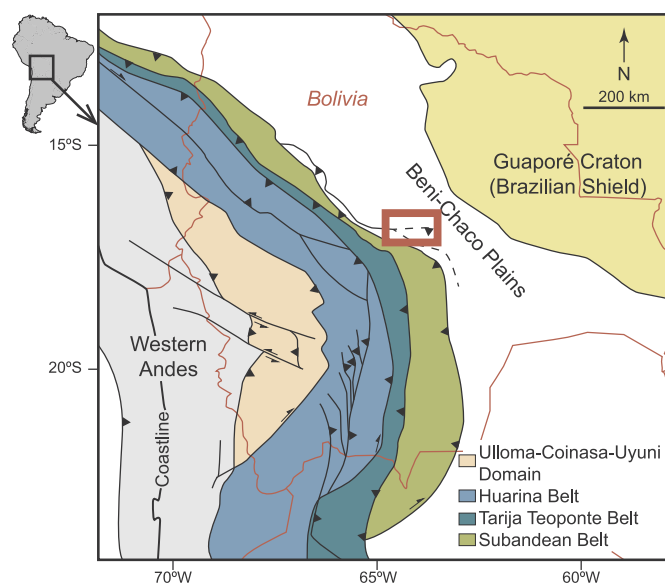


**Fig. 1.** Tectonic map illustrating the main structural units surrounding the Boomerang Hills (modified from *Geobolivia*, 2000). Red rectangle: study area displayed in *Figs. 2, 4, 5, 18 and 19*. (For interpretation of the references to color in this figure legend, the reader is referred to the Web version of this article.)

paleomagnetic rotation data, and concluded that the motion component perpendicular to the orogen increases in the region near the Andes bend, whereas the parallel component increases as one moves away from it. *Baby et al. (1994)* and *Giraud and Limachi (2001)* determined how the basement configuration and the Paleozoic sequence wedge affected the structure development, and they pointed out that the absence of a sufficiently thick Paleozoic sequence induced the Andes bending. *Hinsch et al. (2002, 2003)* studied how the obliquity of the basement with respect to the general shortening direction affected the position of the deformation front and caused both a deformation partition and a reorganization of the main stress direction. They also showed the importance of the old basement faults and other irregularities on the nucleation of new faults. *Husson and Moretti (2002)* characterized the thermal regime along the Bolivian Andes and their spatial variations, determining an increase towards the Boomerang region. According to these authors active tectonics in the Bolivian Subandean region causes important variations in the regional thermal field. Finally, *Moretti et al. (2002)* modeled the possible fluid migration and the influence exerted by the porosity and textural characteristics of the rocks and other factors, such as the thickness and features of the fault zones.

Understanding the main characteristics of the structures, their distribution and their evolution through time, as well as the distribution of the different stratigraphic units and their thickness variations with time, were the first aims of the present work. This allowed us to gain insight into the influence exerted by the older stratigraphic successions and structures on the features of the different types of structures developed during younger events, both at individual structure scale and at the scale of this portion of the Andean Cordillera. In addition, it allowed us to visualize the distribution of the findings of different types of hydrocarbons in relation to the different types of structures and their location within the region. In order to achieve these objectives, time seismic profiles and 3D volumes were geologically interpreted with the constrain of well data, and subsequently they were used to create geological cross-sections, maps, a structural map and a 3D model. A synthetic cross section, constructed by projecting the closest geological interpretations onto a chosen plane, maps and the 3D model were depth-converted, sequentially decompacted using functions created specifically for the stratigraphic units present in this region, and sequentially restored using kinematic and mechanical algorithms.

## 2. Geographical and geological setting

The studied area, which covers an extension of about 7000 km<sup>2</sup>, is the Boomerang Hills, central Bolivia. From the geological point of view, this area is located in the Beni-Chaco Plain, i.e. the foremost zone of the compressive Andean belt (*Fig. 1*). To the southeast of the Boomerang Hills the Andes bend forming a concave arch towards the southwest, whereas to the west of the Boomerang Hills the Andes form a convex arch towards the southwest. However, the main structures of the Boomerang Hills do not follow any of these directions, instead, they strike approximately W-E. This orientation seems to be controlled by the inherited basement configuration and the distribution of the cover (Silurian to Cenozoic) sequence (*Baby et al., 1994; Welsink et al., 1995a; Giraud and Limachi, 2001; Hinsch et al., 2003*). Moreover, a transition from a southern domain, with dominant shortening of Andean age, to a northern domain, with preserved extensional structures of pre-Andean age, has been documented in this region (*Welsink et al., 1995a*).

The Boomerang Hills have undergone several tectonic episodes from Paleozoic to recent times. As a consequence, structures developed in extensional and contractional settings, as well as some structures that exhibit evidence of successive reactivations, coexist. The deposition of a thick marine sequence of Cambrian-Ordovician age which, together with Precambrian rocks configure the basement (Brazilian Shield), was interrupted in late Ordovician times causing an unconformity in between the Ordovician and Silurian (*Lindquist, 1998*). During the Silurian, a rifting took place, inducing the establishment of anoxic marine conditions favorable to the deposition of shaly source rocks (*Lindquist, 1998*). Several kilometers of marine sediments accumulated during the Devonian, such as Devonian shale source rocks, as well as sandy beds that may act as reservoirs. The sedimentation continued with Carboniferous glacial deposits formed by alternations of shaly and sandy beds that can be source and reservoir rocks respectively (*Baby et al., 1995*). Permian-Triassic rocks are absent, as well as part of the Paleozoic succession. Thus, the middle-upper Mesozoic succession lays unconformably over Paleozoic rocks, and it is mainly formed by shales with interbedded siltstones and sandstones deposited under continental conditions (*Welsink et al., 1995a*). New normal faults developed during Mesozoic and older ones were reactivated under this extensional regime. During Cenozoic times, conglomerates, sandstones and shales were deposited in continental environments. Although a few normal faults were generated and old ones were reactivated at the beginning of the Cenozoic, the tectonic setting changed radically with the initiation of the Andean orogeny and the establishment of a contractional regime responsible for thrusting and reverse reactivation of older normal faults (*Welsink et al., 1995a*).

## 3. Available data

The available data consists of two 2D seismic surveys, the Sara and Palacios Norte, including respectively 213 and 9 time pre-stack seismic lines, two 3D time seismic volumes (Sara Boomerang and Los Penocos) and 31 wells distributed in 18 clusters (*Fig. 2*). These subsurface data were acquired by the oil companies Yacimientos Petrolíferos Fiscales Bolivianos (YPFB)-Andina and Maxus between the 60's and 2000's, who made many hydrocarbon discoveries.

The Sara seismic survey covers the whole study area, whereas the Palacios Norte seismic survey covers the central portion of the study area. Most seismic lines display a N-S or a NE-SW trend, although a few E-W and scarce NW-SE are also available (*Fig. 2*). Commonly, they have a record length of 4000–5000 ms. The total length of all these seismic lines is approximately 3900 km.

The 3D seismic volume called Sara Boomerang, located in the central-southwest part of the study area, is elongated in ENE-WSW direction and recorded 6000 ms (*Fig. 2*). The 3D seismic volume called Los Penocos, located in the northeast sector of the study area, is elongated

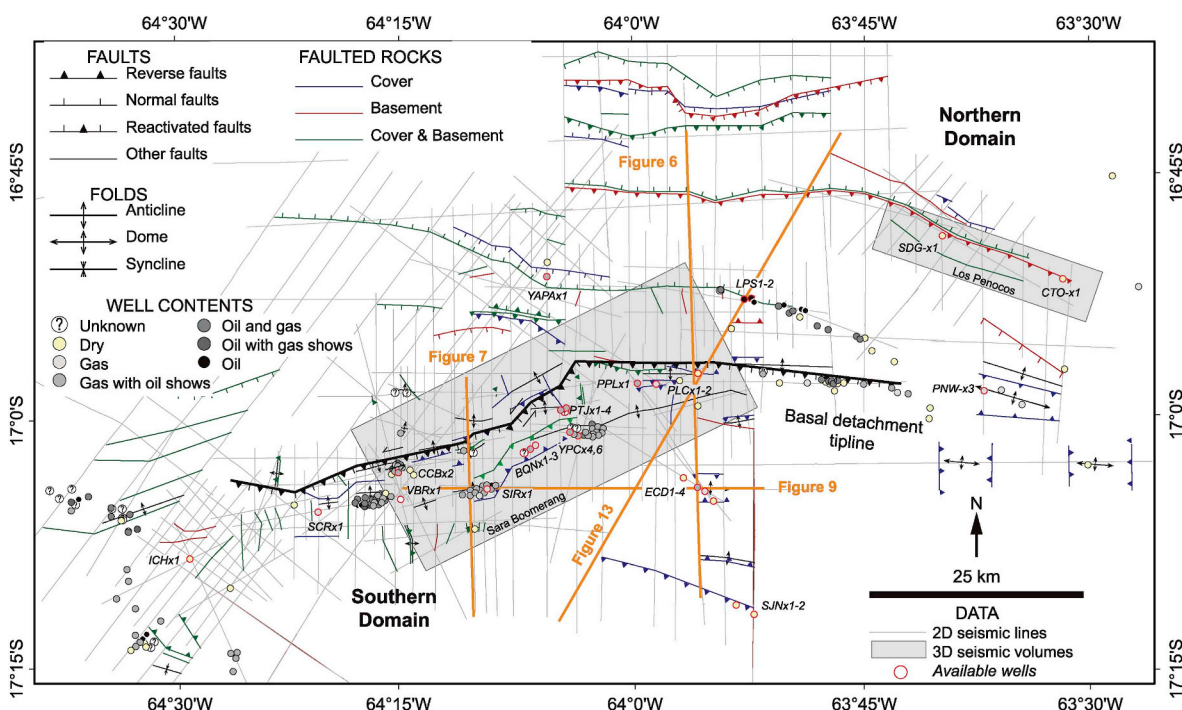


**Fig. 2.** Distribution of the available seismic surveys (lines and volumes) and wells superimposed on a structural map of the study area (see location of the study area in Fig. 1). The map shows the intersection between the topographic surface and the structural elements of outcropping structures, as well as the intersection between the topographic surface and the vertical projections of the structural elements of buried structures. The geographical coordinates and hydrocarbon contents of the wells have been extracted from the IHS Markit Well Database (<https://ihsmarkit.com/products/international-well-data.html>). The names of the available wells are: ICH: Ichoa, VRB: Víbora, CCB: Cascabel, SIR: Sirari, BQN: Boquerón, YPC: Yapacani, YAPA: Yapa, PJT: Patuju, PPL: Puerto Palos, PLC: Palacios, ECD: Enconada, LPS: Los Penocos, SJJ: San Juan, SGD: Santo Domingo, PNW: Palometas noroeste, and CTO: Cuatro Ojos. Víbora, Cascabel, Palacios, Enconada, San Juan and Palometas correspond to the names of the drilled anticlines. The location of Figs. 6, 7, 9 and 13 is shown.

in ESE-WNW direction and recorded 2500 ms (Fig. 2). Both 3D volumes cover an area of 630 km<sup>2</sup>. A total of 93 inlines and crosslines belonging to the two 3D seismic volumes were interpreted from the geological point of view, which makes a total of approximately 800 km. The quality of the seismic imaging of 3D volumes is similar to that of 2D seismic lines.

Most available wells are placed in the central-southern part of the study area (Fig. 2). Wells are much scarcer to the north, except for a couple of wells located in the area covered by Los Penocos 3D seismic volume. The depth of the wells ranges between 1.7 and 1.8 km at SDG-x1 and LPS-1 to LPS-4, around 4 km at SCR-x1, VBR-x1, SIR-x1 and ICH-x1, and reaches almost 5 km at SJJNx2 (south). Wells provided fundamental information in order to identify stratigraphic units within the seismic data, to obtain a velocity model using interval velocities, to carry out the depth conversion and to estimate the parameters necessary for decompacting the stratigraphic succession.

Three main geological elements have been interpreted on the time seismic lines and 3D volumes using the software Kingdom Suite© and Petrel©: tops of selected seismic-stratigraphic units, main faults and main fold axial surfaces. The correlation between the stratigraphic horizons drilled in the wells and the reflectors in the seismic data is based on three types of data included in the confidential well reports elaborated by the company YPFB-Andina: 1) time versus depth tables and/or functions, 2) time values of the different stratigraphic horizons drilled, and/or 3) zooms of interpreted seismic lines in which the wells, along with the drilled stratigraphic horizons, are shown.

#### 4. Stratigraphy

##### 4.1. Stratigraphic units

The stratigraphic succession of the Boomerang Hills has been

divided here in five mega-sequences bounded by major unconformities, which from top to bottom are: Cenozoic, Mesozoic, Carboniferous, Silurian-Devonian and pre-Silurian (modified from Welsink et al., 1995a) (Fig. 3). The Cenozoic, Mesozoic, Carboniferous and Silurian-Devonian successions are cover rocks, whereas the pre-Silurian succession is considered basement. Using the available well data, up to eleven stratigraphic units were identified and used to carry out the geological interpretation of the seismic data: Chaco, Yecua and Petaca fms. (Cenozoic); Cajones, Yantata and Ichoa fms. (Mesozoic); Carboniferous; Iquiri, Limoncito, Roboré and Boomerang fms. (Devonian); Kirusillas Fm. (Silurian); and pre-Silurian (usually considered Precambrian-Ordovician).

A brief description of the lithologies included in these stratigraphic units, based on well data, is given below from younger to older units. The main seismic-stratigraphic features are described in Welsink et al. (1995a). The Cenozoic mega-sequence is formed by three continental, siliciclastic formations. The Chaco Fm. (Cenozoic) consists of an alternation of sandstones and shalier units; sandstones predominate in the upper part, and limolites and shales are the main constituent of the lower part. The Yecua Fm. (Cenozoic) is made up of claystones with sporadic sandy intercalations more frequent towards its base. The Petaca Fm. (Cenozoic) is constituted by sandstones and shales in variable proportions, although in general, the upper part is sandier, whereas shales dominate the lower section. Three continental-shallow marine, siliciclastic formations, including chert and gypsum horizons, constitute the Mesozoic mega-sequence. The Cajones Fm. (Cretaceous) is a fine to coarse sandy unit with intercalations of shalier intervals as well as calcarenites. This unit appears sporadically in the study area, which prevented its tracking on the seismic data and obtaining a surface useful for restoration and decompaction. The Yantata Fm. (Cretaceous) is formed by sandstones with less shaly intercalations than the units above, although they may be relatively important towards its top; chert

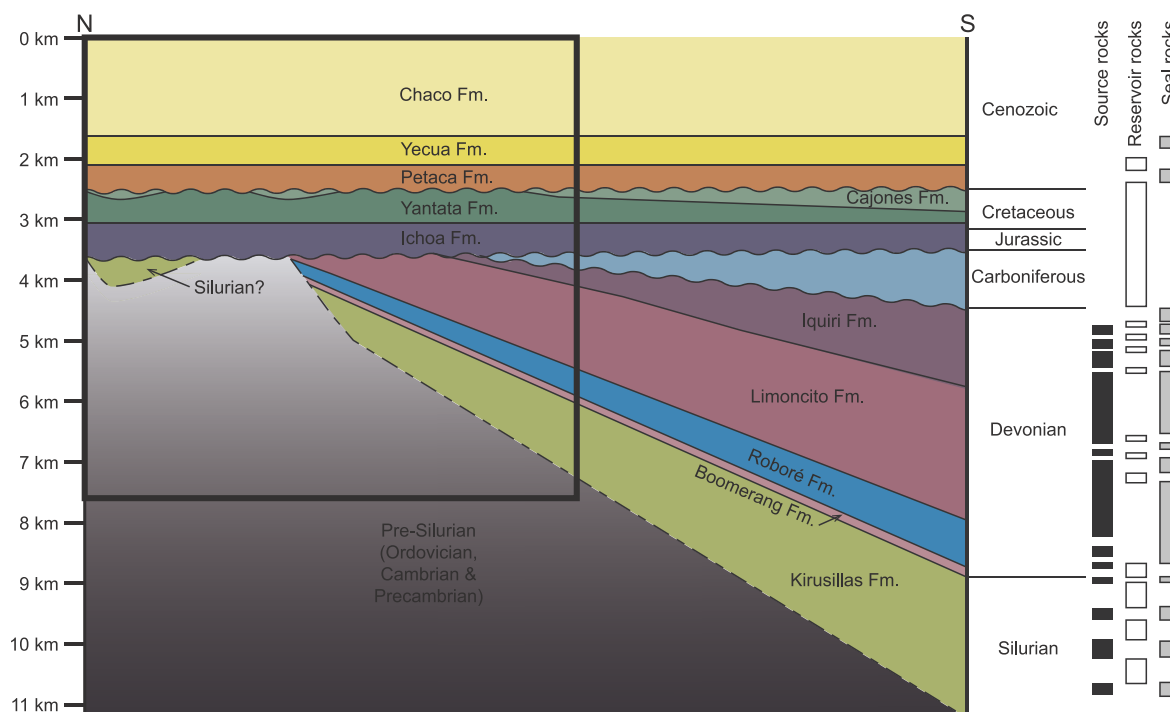


**Fig. 3.** Simplified stratigraphy of the Boomerang Hills and surrounding areas showing the geometry of the different units, their ages and the location of the potential source rocks, reservoir rocks and seal rocks (modified from Baby et al., 1995). The angle between the Mesozoic and Paleozoic rocks has been exaggerated for better visualization. Black square: study area, wavy lines: erosive unconformities, dashed lines: unconformities without evidence of erosion.

horizons used as key beds occur within this unit. The Ichoa Fm. (Cretaceous-Jurassic) is a sandy sequence that contains interbedded shales, mudstones and gypsum levels. The Carboniferous unit is a continental mega-sequence made of sandstones with some intercalations of limestones, limolites and gypsum. The Silurian-Devonian mega-sequence includes five marine, siliciclastic units with limestones concentrated in the lower part. The Iquiri Fm. (Devonian) consists of two shaly intervals separated by fine-to very fine-graded sandstones. Since it only appears in the southernmost well, it was not interpreted on the seismic data and, therefore, was not considered for the restoration and decompaction. The Limoncito Fm. (Devonian) is a shaly unit with thin intercalations of fine-grained sandstones. The Roboré Fm. (Devonian) is mainly formed by sandstones. The Boomerang Fm. (Devonian) is a shaly level ascribed to the base of the overlying unit in some wells. The Kirusillas Fm. (Silurian) consists of an alternation of limestones, shales and sandstones topped by a sandstone bed. The pre-Silurian mega-sequence is made up of a marine Cambrian-Ordovician succession formed by quartzites with shale fragments, and Precambrian rocks.

Seismic and well data show that the Mesozoic and Cenozoic mega-sequences appear everywhere in the study area (Fig. 3). The thickness of the Cenozoic mega-sequence is around 1.2 km in the northeast part of the study area (SDG-x1, CTO-x1 and SIG-x1 wells) and more than 3.5 km in the southwest (ICH-x1 well), although its total thickness is unknown given that the succession top is eroded. The Cenozoic base is a paraconformity over the Mesozoic. The Mesozoic mega-sequence displays an approximately constant thickness of almost 850 m all over the study area (Fig. 3), except for some localities where Mesozoic rocks fill in depressed blocks, in some cases bounded by faults. The base of the Mesozoic is an erosive angular unconformity that truncates progressively older rocks towards the north from the Carboniferous to the pre-Silurian mega-sequences (Figs. 3 and 4), and whose angle with the underlying units is up to 10° increasing to the north. The Carboniferous and Silurian-Devonian mega-sequences display an irregular distribution along the studied area. They are almost absent in the north portion of the study area, where only small remnants of the Silurian-Devonian mega-sequence may be found in depressed regions controlled by

downthrown fault blocks (Fig. 3). In the south part of the studied region, the Silurian-Devonian and the Carboniferous mega-sequences have a wedge shape, thickening towards the south and reaching a total thickness of up to around 8 km. The base of the Carboniferous is an angular unconformity over the Silurian-Devonian rocks. The top of the pre-Silurian mega-sequence in the south portion of the study area is an inclined unconformity where the lower part of the Silurian-Devonian mega-sequence onlaps, whereas it is roughly flat-lying in the north part of the study area.

#### 4.2. Mechanical stratigraphy and tectonics-sedimentation relationships

Two units are recognized in the south part of the study area taking into account how the rocks reacted to deformation: an upper unit formed by the Cenozoic, Mesozoic, Carboniferous and Silurian-Devonian mega-sequences, and a lower unit formed by the pre-Silurian mega-sequence (Fig. 3). The differentiation of these two units is based on: 1) the fact that the structures developed in the upper unit are different (mainly folds and faults) and more abundant than those developed in the lower unit (mainly faults), and 2) the occurrence of a significant detachment along Silurian ductile rocks separating the upper and lower units. The different behavior of these two units is probably due to a rheological control that caused the upper unit, formed by shales, sandstones and some limestones and gypsum, to behave in a relatively ductile manner, while the lower unit, constituted mainly by quartzites, behaved more rigidly. On the other hand, the high viscosity contrast between the Silurian shales, located at the base of the upper unit, and the underlying Ordovician quartzites gave rise to a detachment.

Regarding the tectonics-sedimentation relationships, most of the Cenozoic rocks (Chaco and Yecua fms.) correspond to a post-extension, pre-inversion succession. It is debatable whether the youngest sediments of the Chaco Fm. show evidence of syn-tectonic sedimentation related to contractional/inversion folds, but unfortunately, the shallow part of the seismic data is poorly imaged. The lowermost Cenozoic sediments (Petaca Fm.) belong to a syn-extension succession (see also

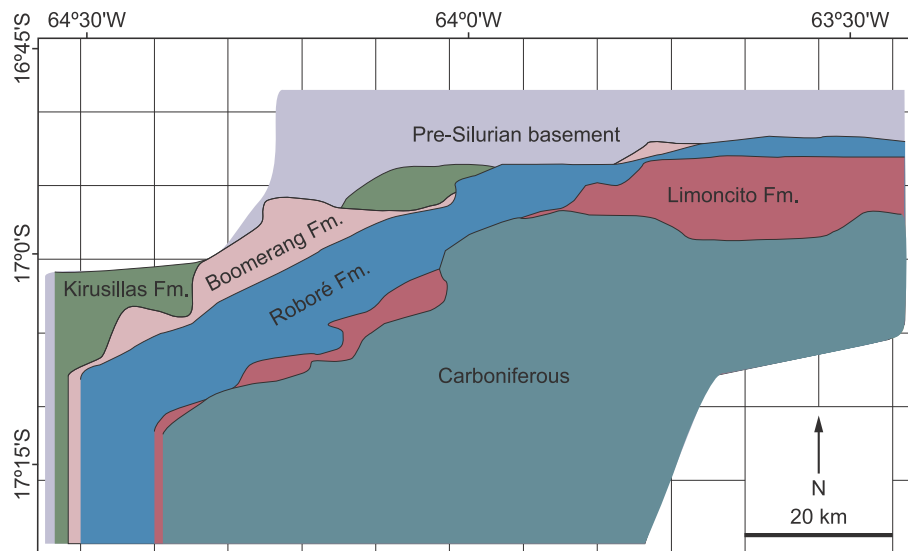


**Fig. 4.** Sub-crop map under the Mesozoic unconformity in the study area (see location of the study area in Fig. 1). The Mesozoic rocks lay on top of progressively older Paleozoic rocks towards the north. Uncolored regions correspond to areas where no data are available.

Welsink et al., 1995a). Most of the Cretaceous rocks (Cajones and Yantata fms.) consist of a pre-extension succession regarding the lowermost Cenozoic and a post-extension succession with respect to the lowermost Cretaceous and Jurassic rocks (Ichoa Fm.), which are considered as a syn-extension succession (see also Welsink et al., 1995a). The relationships between tectonics and the Carboniferous and Devonian sediments (Carboniferous, Iquiri, Limoncito, Roboré and Boomerang fms.) are unclear, although they may belong to a pre-extension succession with respect to the Jurassic-lower Cretaceous succession, and to a post-extension succession with respect to Silurian sediments (Kirusillas Fm.) considered as a syn-extension succession (see also Welsink et al., 1995a). The upper part of the Cambrian-Ordovician rocks would be a syn-extension succession, whereas the lower part of the Cambrian-Ordovician and the Precambrian rocks may correspond to a pre-extension succession.

## 5. Main structural elements

According to the geological interpretation of the seismic data, the studied area includes folds as well as normal, reverse, oblique and reactivated faults. Some of these structures affect only the basement, whereas others are developed in the cover and others involve both units. Structural maps of the study area (Figs. 2 and 5) show that most of the main or, at least, larger structures exhibit a general E-W orientation, although some structures strike ESE-WNW in the eastern sector, whereas they tend to be ENE-WSW in the southwestern sector. The disparities between the north and south portions of the studied area led Welsink et al. (1995a) to differentiate two domains, separated by a major tectonic structure, whose main structural characteristics are described below.

### 5.1. Structure of the southern domain

The maps in Figs. 2 and 5 show that most of the structures in this domain are developed either within the cover rocks, or within the cover and basement, and only a few involve solely the basement.

One of the most prominent structural features of this domain is a basal detachment (Mingramm et al., 1979; Baby et al., 1989; Dunn et al., 1995; Kley, 1999) of, at least, 80 km along-strike length, placed mainly within the shales of the lowermost part of the cover rocks (Silurian), close and subparallel to the boundary with the pre-Silurian basement. According to Giraud and Limachi (2001), the basal

detachment in the Boomerang Hills corresponds to the basal detachment of the Andean Cordillera. The orientation of the detachment tip line varies from E-W to the west of the study area, to ENE-WSW in the central portion, to E-W towards the east (Figs. 2 and 5). The detachment tip line follows tightly the zone where the basement top changes from dipping to the S or SE (south part of the study area) to be sub-horizontal (north part of the study area). The average strike of the detachment, and that of the basement top, in the southern region is E-W dipping gently to the S. The dip of the basal detachment is not constant everywhere; thus, it is gently waved in some areas due to basement irregularities of the order of 3–4 km width, interpreted as old basement faults and/or Silurian normal faults (Laffitte et al., 1998). The basal detachment climbs up section near its termination and exhibits a reverse offset in the Mesozoic and Cenozoic mega-sequences (Fig. 6). However, the cut-off point of the Silurian-Devonian boundary on the detachment hangingwall is deeper than its footwall equivalent point denoting that the detachment behaved as a normal fault. The normal motion probably took place after Silurian-Devonian sedimentation because these rocks do not exhibit syn-extensional features and before Mesozoic sedimentation, while reverse fault reactivation occurred during Cenozoic times. Despite the reverse motion along the basal detachment, Devonian and Silurian hangingwall rocks are still sunk with respect to their footwall equivalent rocks (i.e. part of the normal motion is preserved) indicating mild inversion tectonics.

The shortening in the frontal part of the basal detachment, i.e. in the zone where the basement dip changes from dipping gently to the S to sub-horizontal, is accommodated by two different types of kilometer-scale structures, which constitute the northern boundary of the southern structural domain: 1) thin-skinned tectonic wedges (include back-vergent structures) (Fig. 6), and 2) thin- and thick-skinned folds and faults (all the structures verge towards the tectonic transport sense) (Fig. 7).

Tectonic wedges occur for almost 10 km along strike in the central portion of the study area, where the tip line of the basal detachment strikes E-W (Figs. 2 and 5). Two different types of frontal tectonic wedges occur along strike: 1) Tectonic wedges that accommodate all the shortening (Fig. 8a), and 2) tectonic wedges where the shortening is partially accommodated by the wedge and part is transferred to the north through and upper detachment (Fig. 8b). In the second case, the basal detachment near its termination becomes a hangingwall ramp that cuts off the Silurian-Devonian succession developing a fault-bend fold, and farther north it becomes an upper detachment that runs along

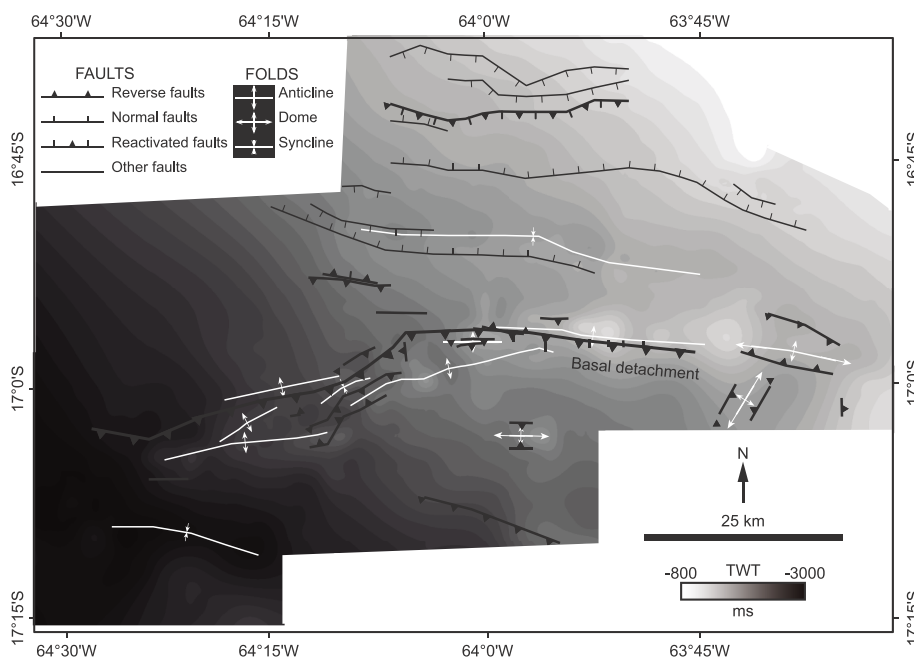


**Fig. 5.** Structural map of the Ichoa Fm. in the study area (see location of the study area in Fig. 1) showing the most important folds and faults that affect this stratigraphic unit. See the stratigraphic position of the Ichoa Fm. in Fig. 3.

the Mesozoic unconformity and places Mesozoic and Cenozoic rocks in a hangingwall flat situation on top of Silurian or pre-Silurian rocks in a footwall flat situation. In both types of tectonic wedges, the backthrust, whose maximum S-directed displacement is approximately 1.3 km, propagates through the Mesozoic and the lower part of the Cenozoic succession in a hangingwall ramp over footwall ramp situation causing an open ramp anticline developed on the backthrust hangingwall, whose geometry resembles that of shear fault-bend folds (Suppe et al.,

2004). The development of one or another type of tectonic wedge is controlled by the spatial distribution of the Silurian ductile rocks near the basal detachment tip. The first mode developed in those areas where the Silurian ductile rocks pinch out against the south dipping basement (Fig. 8a). The second mode takes place when the Silurian ductile rocks exceed the boundary between the S-dipping and sub-horizontal basement (Fig. 8b).

In the easternmost and western portions of the study area where the

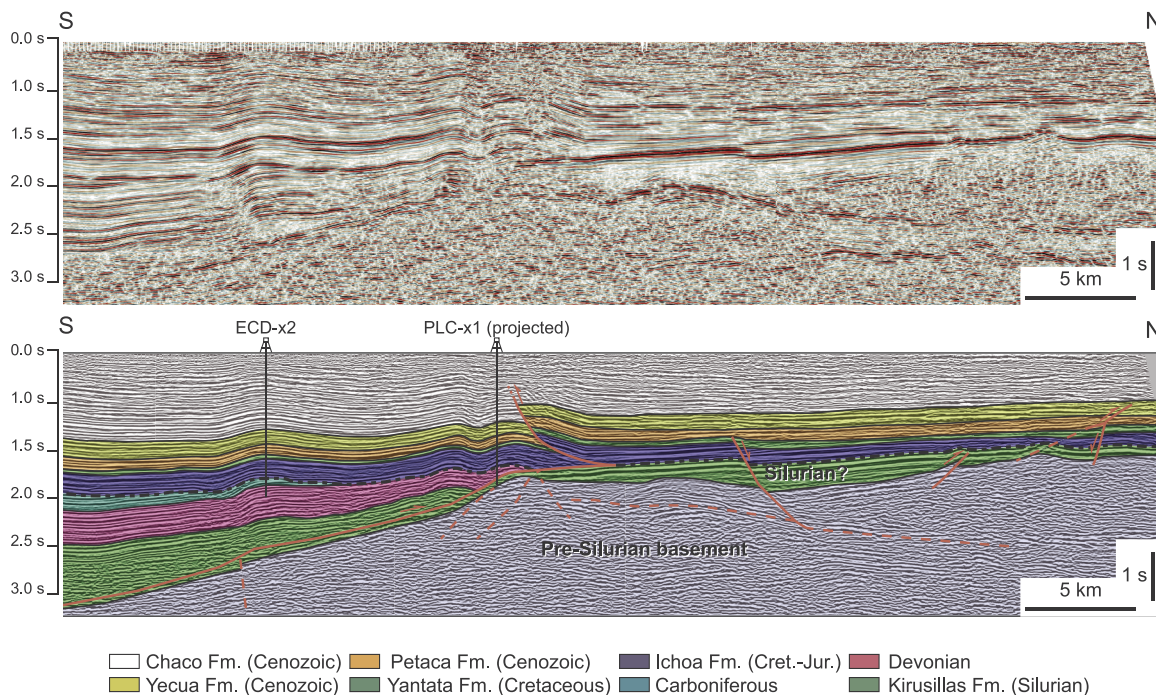


**Fig. 6.** Geological interpretation of a seismic line in the central-eastern part of the study area illustrating the boundary between the southern (mainly compressive and thin-skinned) and the northern (dominantly extensional and thick-skinned) domains. A backthrust emanates from the basal detachment termination forming a tectonic wedge. A north-dipping normal fault in the northern domain offsets the Pre-Silurian, Silurian, Devonian and Mesozoic mega-sequences and exhibits a thicker Petaca Fm. in its hangingwall than in its footwall which suggests that fault activity took place during Early Cenozoic. PLC: Palacios well drilling the Palacios anticline and ECD: Enconada well drilling the Enconada anticline. See location in Fig. 2.

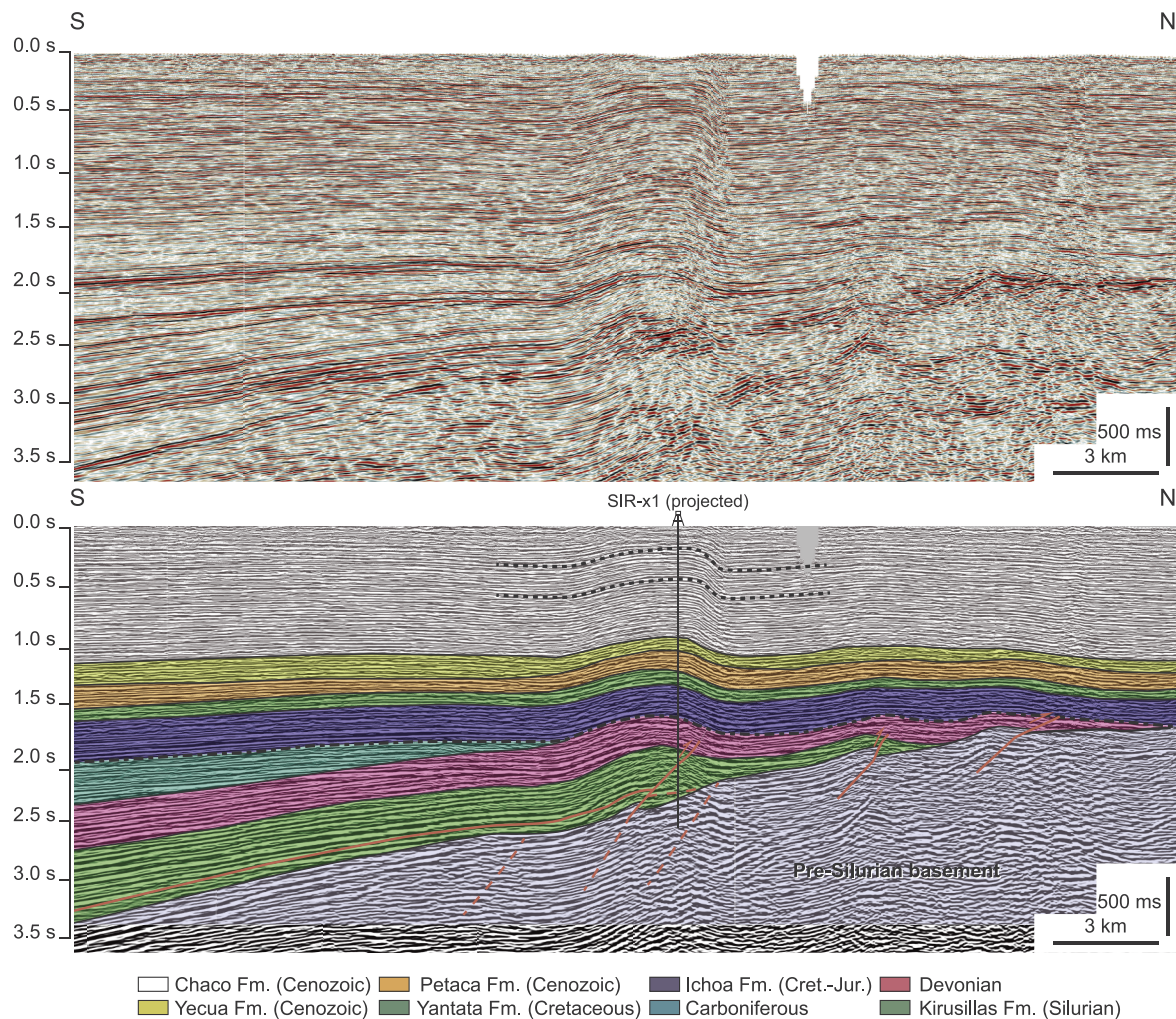


**Fig. 7.** Geological interpretation of a seismic line in the central-western part of the study area showing the boundary between the southern (mainly compressive and thin-skinned) and the northern (dominantly extensional and thick-skinned) domains. N-directed reverse faults and folds develop near the termination of the basal detachment. SIR: Sirari well. See location in Fig. 2.

tip line of the basal detachment strikes E-W and ENE-WSW respectively (Figs. 2 and 5), the frontal termination of the basal detachment forms two types of fold/fault structures for almost 70 km along strike: 1) folds in the hangingwall of reverse faults, developed in the vicinity of the basal detachment tip, that cut and offset the lowermost portion of the cover and basement rocks located below the basal detachment (Fig. 8c); and 2) cover rock folds developed near the tip of the basal detachment (Fig. 8d). In the first case, the reverse faults dip steeply and the fold backlimbs are oblique to the faults (Fig. 8c). In the second case, the thrust faults dip moderately and the fold backlimbs are approximately parallel to the thrust. Both types of folds are N-vergent and open structures, and both types of faults dip to the south, are N-directed and their displacements do not exceed 150–200 m.

Frontal tectonic wedges developed only in those areas where the basal detachment strikes E-W and where the Silurian-Devonian rocks onlap abruptly on the basement top. In these regions the boundary between the S-dipping and the sub-horizontal basement top is a narrow, angular zone, i.e. a kink-like hinge. The absence of favorable ductile Silurian shales, where the basal detachment is located, inhibited the forward propagation of the detachment and triggered the development of a backthrust developing a tectonic wedge (Figs. 6, 8a and 8b). In contrast, frontal fold/fault structures developed where the onlap of the Silurian-Devonian rocks on the basement top is smooth. In these regions the boundary zone between the S-dipping and the sub-horizontal basement top is a wide, smooth zone, i.e. a rounded-like hinge (Figs. 7, 8c and 8d).

Apart from the basal detachment and their related frontal structures, other structures occur within this domain. There are also some E-W and ENE-WSW striking faults, usually steeply to moderately dipping to the S although some N-dipping faults also occur, that may reach 10–15 km along-strike length. These faults are interpreted as old normal faults affecting the basement. Some of them have been partially reactivated and propagated up section forming folds, which might be interpreted as forced folds, affecting all the cover rocks. Their maximum reverse displacement is approximately 200–300 m (basement faults in Fig. 2).

Not all the structures developed in the southern structural domain follow the general E-W trend; thus, some faults strike approximately N-S and dip steeply both to the E and to the W (Fig. 2). These faults may reach almost 7 km along-strike length, exhibit maximum displacements of approximately 150–200 m and, although they usually only affect the basement, some of them involve up to the Cenozoic rocks. Their movement sense is unclear, although some seem to display a reverse sense of motion.

Short anticlines along strike, whose periclinal terminations are very close and remind elongated domes, occur in some localities. These relatively symmetrical, open structures, exhibit kilometer-scale dimensions and are well developed in the cover rocks (Figs. 2 and 5). The internal structure of some of these structures may include steep, reverse faults with a very small displacement that affect the lowermost part of the cover (Silurian and Devonian); it is unclear whether they involve

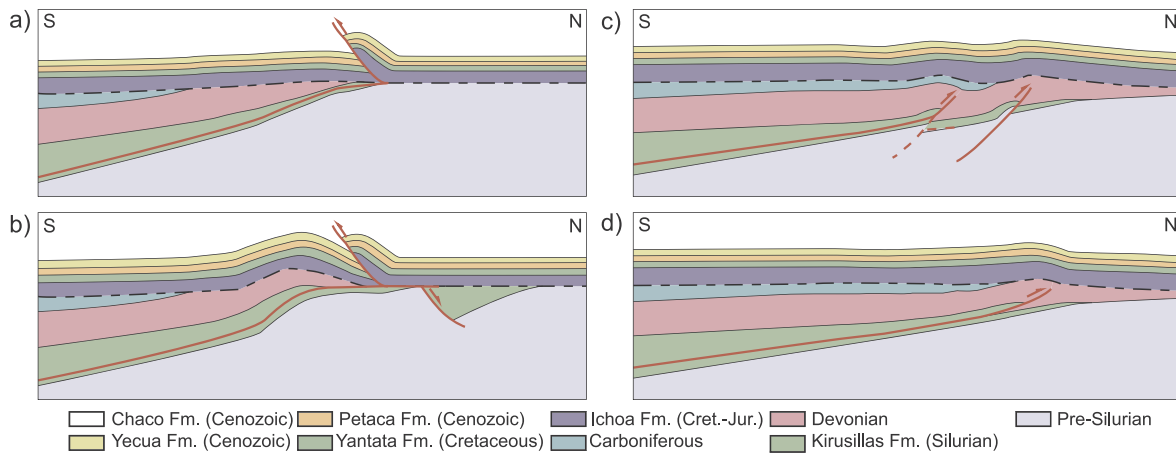


**Fig. 8.** Simplified models simulating the principal terminations of the basal detachment in the Boomerang Hills: a) tectonic wedge where the backthrust emanates from the basal detachment tip located within a Silurian pinch out, b) tectonic wedge where the backthrust emanates from an upper detachment that terminates above a half-graben filled in by Silurian rocks, c) folds related to steeply dipping faults that involve basement rocks, and d) folds related to gently dipping faults developed within cover rocks.

the basement (Fig. 9). These faults dip to the interior of the anticlines and run mainly along the anticline limbs, and sporadically offset the anticline crests. Some anticlines display a box-type geometry with a flat crest in the lowest horizons, whereas they become open rounded folds in the highest horizons.

Thus, except for some faults that only affect basement rocks, which could have been active during Paleozoic times (pre-Andean), the age of the deformation in the southern domain is mainly Upper Cenozoic (Andean) because these rocks, deposited during the Andean cycle, are the youngest ones involved in the structures.

### 5.2. Structure of the northern domain

Unlike in the southern domain, most of the structures in the northern domain involve both the basement and the cover or only the basement, and just a few structures affect only cover rocks (Figs. 2 and 5).

The most abundant structures are E-W trending normal faults steeply to moderately dipping both to the N and to the S. These faults can reach more than 60 km along-strike length and their maximum displacement is approximately 300–400 m. The thicker hangingwall successions with respect to their footwall equivalents (syn-extension sediments), as well as the age of the faulted rocks, indicate that some faults were active growth faults during Cambrian-Ordovician times (structures within the basement), others during the middle part of the Mesozoic, and others during the early Cenozoic (Fig. 6). Some normal faults bound remnants of rocks of probably Silurian age, surrounded by basement rocks but do not offset the erosional unconformity at the base of the Mesozoic; this suggests that they were active during Paleozoic times and stopped before the Mesozoic erosion. Some normal faults exhibit a listric geometry and open anticlines developed in their hangingwalls, interpreted as rollover anticlines.

Three principal modes of inversion tectonics have been identified, all of them involving Mesozoic normal faults: 1) Mesozoic normal faults reactivated as normal faults during early Cenozoic (Fig. 10a), 2) Mesozoic normal faults reactivated as reverse faults during Cenozoic (Fig. 10b), and 3) Mesozoic normal faults cut and offset by Cenozoic thrust faults (Fig. 10c). In the first case, the faults show syn-extension sediments of two different ages (Jurassic-lowermost Cretaceous and lowermost Cenozoic) separated by a post-extension sequence with respect to the underlying sediments and pre-extension with respect to the overlying sediments. In the second case, the faults exhibit reverse displacement when involving Cretaceous and Cenozoic rocks, but normal displacement still preserved in the lowermost Cretaceous-Jurassic and

Paleozoic rocks. The last two cases correspond to a mild positive inversion tectonics (usually less than 100 m of fault displacement measured in Cenozoic rocks).

A few E-W trending, S-dipping thrusts, of a few hundred meters along-strike length, have been also mapped in this domain. Their N-directed displacements may reach around 50 m and they offset only cover rocks.

Moreover, a few open to gentle folds, developed in cover rocks, are mainly located in the south part of this domain. They exhibit sub-vertical axial surfaces and fold traces that reach a few hundred meters along strike.

Thus, most of the structures in this domain developed from Paleozoic to Early Cenozoic (pre-Andean times), except for reactivations of normal faults as reverse faults, thrusts and folds that developed during Cenozoic (Andean times) because these rocks are the youngest ones affected by these structures.

From the description of the structures above, we conclude that there are important differences between the northern and southern structural domains in terms of structural style, types of structures, tectonic regime responsible for the structures, age of the structures, basement disposition and involvement in the structures, and stratigraphic units and thickness (Table 1).

### 5.3. Tectonic transport vector

The Andean vector of tectonic transport in the study area and surroundings has been measured using GPS velocities of plate current movements (Bevis et al., 2001; Hindle et al., 2002), bed-length restorations for different time periods (Hindle et al., 2002), surface restorations (Hinsch et al., 2003), and measurements of kinematic indicators on fault populations developed during different times (Mercier et al., 1992; Klosko et al., 2002). The average direction of the tectonic transport vector estimated using previous authors data is N047E. Since the average direction of the tectonic transport vector is NE-SW and the strike of the structures mapped on the seismic data varies from ESE-WNW to ENE-WSW, being E-W an average strike, it is likely that the faults did not behave as purely dip-slip but oblique faults. Thus, the Boomerang Hills were subjected to transpression during the Andean orogeny.

Assuming that the average direction of the tectonic transport estimated is correct and constant in the study area, and knowing the orientation of the basal detachment, it is possible to determine the amount of dip-slip and strike-slip components of the basal detachment motion during Andean times. These components are controlled by both the fault dip and the angle between the fault strike and the tectonic



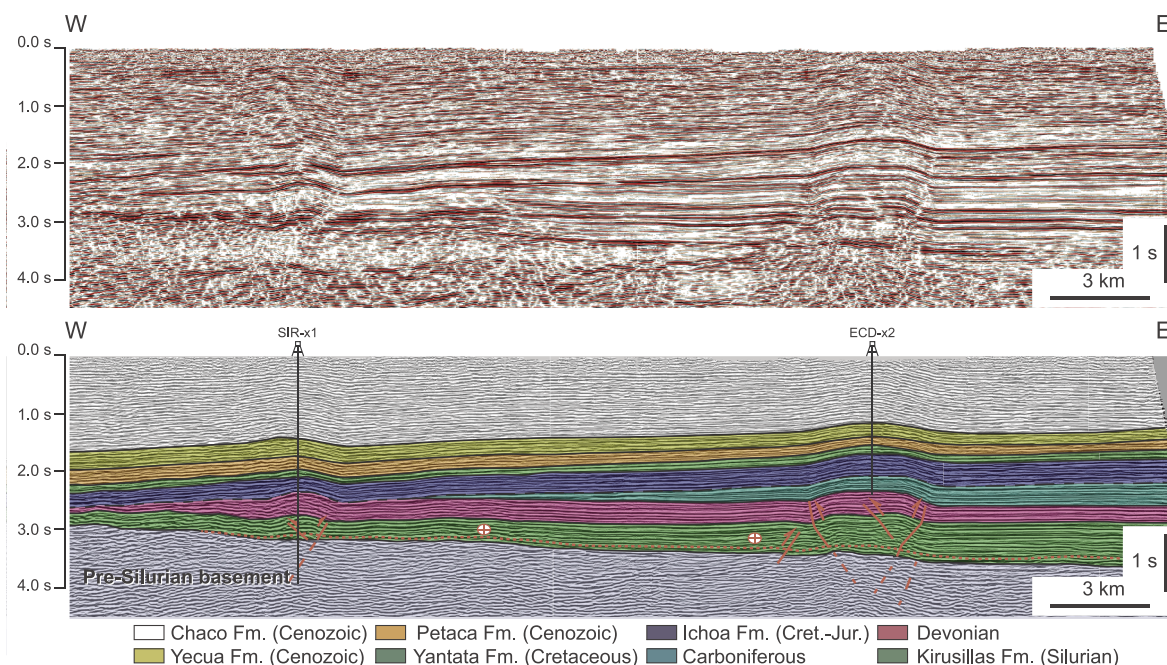


**Fig. 9.** Geological interpretation of a seismic line across the southern domain showing folds whose limbs are cut and offset by faults. ECD: Enconada well drilling the Enconada anticline and SIR: Sirari well. See location in Fig. 2.

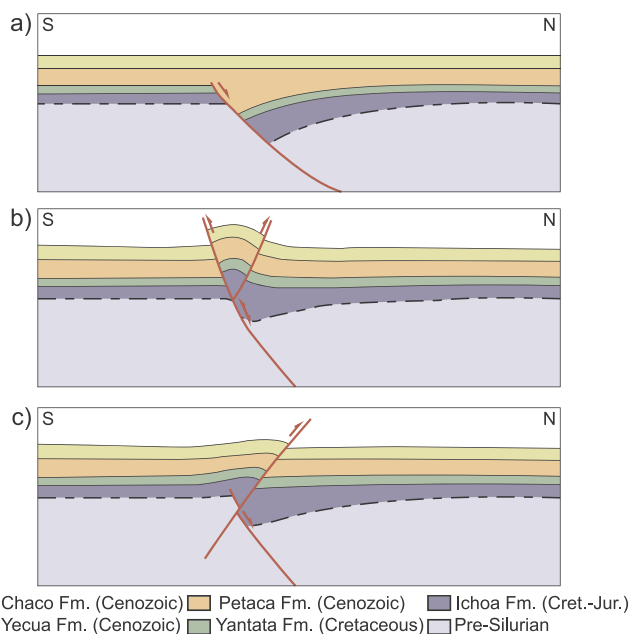


**Fig. 10.** Simplified models simulating the principal modes of inversion tectonics in the northern domain of the Boomerang Hills. Cretaceous-Jurassic normal faults: a) reactivated as normal faults during the lower part of the Cenozoic; b) reactivated as reverse faults during the Cenozoic, so that part of the normal offset is still preserved, and including backthrusts; and c) cut and offset by Cenozoic thrusts that dip in opposite sense to the normal faults.

transport vector (Fig. 11). In general, the percentage of dip-slip component increases as the fault dip and the angle between the fault strike and the tectonic transport vector rise. The true strike and dip of the basal detachment were estimated in two localities using depth-converted seismic data. The angle between the average tectonic transport vector and the strike of the detachment in the eastern part of the studied area, where it strikes approximately E-W, is around 45° and the detachment is subhorizontal. According to the graph (Fig. 11), the detachment behaved as a reverse left-lateral fault because the pitch of the

kinematic indicators would be slightly greater than 45°, i.e. the dip-slip component would be approximately 52% of the total, whereas the strike-slip component would be of the order of 48%. Steeper (around 60° dip) faults with similar E-W strike show pitches of kinematic indicators greater than 60°, and therefore, they would also be classified as reverse left-lateral faults, but their percentages of dip-slip component would be greater, about 70% and, consequently, their strike-slip component would be less than 30% (Fig. 11). The angle between the basal detachment strike in the western part of the study area, where its strike is approximately ENE-WSW, and the average tectonic transport vector is around 15°. This means that the detachment behaved as a left-lateral reverse fault because the pitch of the kinematic indicators would be around 15° (Fig. 11); i.e. the strike-slip component would be approximately 82% of the total, whereas the dip-slip component would be around 18%. This change in the behavior of the detachment along strike is consistent with the model proposed by Hinsch et al. (2002). It is likely that several pre-Andean extensional faults also behaved as oblique faults during the Andean contraction, but in those cases where the faults maintained their normal displacement despite the Andean shortening, then the Andean oblique reactivation went unnoticed.

The termination of the basal detachment as a frontal tectonic wedge has been recognized only in those areas where the basal detachment strikes E-W. This may suggest that this type of structure only developed in regions where the basal detachment acted mainly as a reverse fault, but not in those areas where it had a dominant strike-slip displacement.

Unfortunately, we do not know the orientation of the tectonic transport vector during pre-Andean times. Since extensional events of different ages took place, it is possible that the old tectonic transport vectors had different orientations. In any case, since many pre-Andean structures exhibit E-W strikes, it is likely the existence of approximately N-S tectonic transport vectors perpendicular to the structures.

## 6. Construction and restoration of a 2D cross-section

Since the geological interpretation was done in time, we needed a velocity model to depth-convert the interpretation and the compaction parameters to analyze the thickness variations in the stratigraphic sequences through time.

**Table 1**  
Main differences between the southern and northern structural domains of the Boomerang Hills.

	SOUTHERN DOMAIN	NORTHERN DOMAIN
Main structural style	Mainly thin-skinned	Thick-skinned
Most common type of structures	Folds and faults	Faults
Detachment features	S-dipping, detachment	No detachment
Dominant tectonic regime	Contractional	Extensional
Age of main deformation	Cenozoic	Paleozoic-Early Cenozoic
Main orogenic cycle	Andean	Pre-Andean
Most important pre-Andean structures	Paleozoic extensional detachment	Normal faults
Most important Andean structures	Frontal detachment termination (tectonic wedges and faults/folds)	Reverse reactivation of normal faults, and minor thrusts and folds
Basement top attitude	S-dipping	Sub-horizontal
Geometry of the cover units	Wedge shaped (lower part) and tabular (upper part)	Tabular
Units more frequently involved in the structures	Cover and basement-cover	Basement and basement-cover
Age of the stratigraphic sequence	Basement: Precambrian-Ordovician Cover: Silurian, Devonian, Carboniferous, Mesozoic, Cenozoic	Basement: Precambrian-Ordovician Cover: Silurian (sporadically), Mesozoic, Cenozoic
Thickness of the stratigraphic sequence	Thick	Thin
Tectonic unit	Andes	Beni-Chaco Plain
Most common hydrocarbon	Gas	Oil

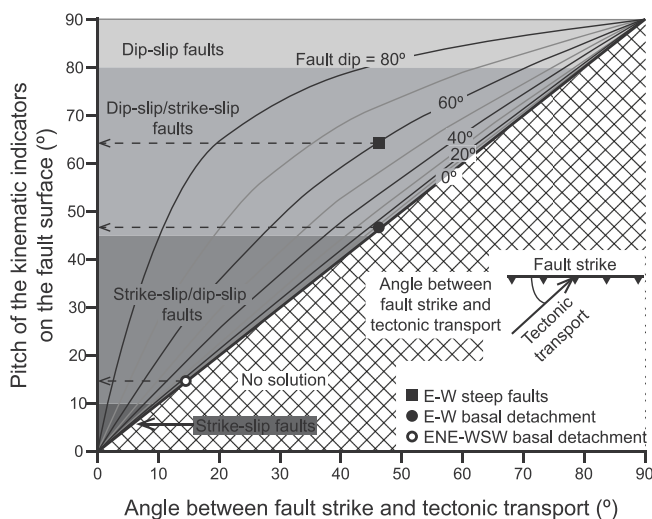


**Fig. 11.** Graph that illustrates the pitch of the kinematic indicators on the fault surface versus the angle between the fault strike and the tectonic transport vector for different fault dips. The values corresponding to three structure types found in the Boomerang Hills are plotted on the graph. To construct this graph, the orientation of the line resulting from the projection of the tectonic transport direction on the fault plane has been calculated (the direction of this line is that of the transport direction and its dip is the apparent dip of the fault plane along that direction), then the angle between the fault strike and this line on the fault plane (i.e. the pitch) has been calculated for different fault dips.

**6.1. Velocity model and depth conversion**

The horizons and surfaces obtained from the geological interpretation of the seismic data were depth converted using the information from ten wells in order to visualize the proper geometry of the structures in both 2D and 3D, as well as to carry out the restoration of a geological cross-section and a 3D geological model. Three types of velocity models were constructed using these values: velocity laws for each well, an average velocity law combining the laws derived from all the wells, and interval velocities for each seismic-stratigraphic unit obtained by averaging the velocities of each unit estimated in the available wells. The models based on velocity laws were not employed because the large variations in the stratigraphic thicknesses of some units throughout the study area would invalidate their use. Therefore, the velocity model, based on interval velocities (Table 2), was selected to carry out the depth conversion, as it should offer the best results given that the boundaries of the different velocity units, i.e.

stratigraphic tops and/or faults, had already been mapped. The depth conversion was carried out using the software Move©. Anyway, we must bear in mind that the depth conversion performed is an approximation.

**6.2. Compaction parameters**

When performing a restoration the stratigraphic units must undergo a certain amount of decompaction as the ones overlying them are removed. The variation of porosity with depth for each stratigraphic unit must be known in order to take compaction into account. This information is usually calculated by fitting the following exponential function through points plotted on porosity versus depth graphs (Eqn 1):

$$\phi = \phi_0 e^{-cy} \tag{1}$$

where  $\phi$  is the porosity,  $\phi_0$  is the initial porosity,  $c$  is the compaction coefficient, and  $y$  is the depth. Seventeen well reports include tables gathering values of porosity and depth for different Cenozoic, Mesozoic, Devonian and Silurian units. The main drawback that arose when trying to find out the exponential functions for each stratigraphic unit was that most of the well data were constrained to narrow depth ranges and did not cover a sufficient depth range to support any particular function (full circles in Fig. 12a). This made difficult the determination of the initial porosity and the compaction coefficient. To sort this out, on depth versus porosity graphs we freehand drew a function (solid line in Fig. 12a) through the average value of the well-data point cloud following a similar path to that of the functions constructed by previous authors for lithologies equivalent to those of the stratigraphic unit to be analyzed (dashed lines in Fig. 12a). To quantify the initial porosity and the compaction coefficient, points at arbitrary, different depths on the

**Table 2**  
Interval velocities calculated for each stratigraphic unit interpreted on the seismic data.

Unit	Velocity (m/s)
Chaco Fm. (Cenozoic)	2531
Yecua Fm. (Cenozoic)	3129
Petaca Fm. (Cenozoic)	3263
Yantata Fm. (Cretaceous)	3227
Ichoa Fm. (Cretaceous-Jurassic)	3446
Carboniferous	4161
Ilmoncito Fm. (Devonian)	3649
Roboré Fm. (Devonian)	4023
Boomerang Fm. (Devonian)	3582
Kirusillas Fm. (Silurian)	4034

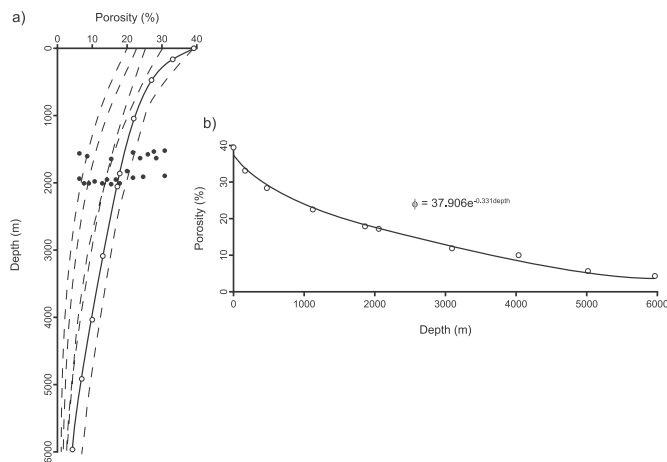


**Fig. 12.** a) Depth versus porosity graph for the Petaca Fm. Full circles: well data, dashed lines: reference curves taken from the literature (Bond et al., 1983; Angevine et al., 1990) for lithologies similar to those of the Petaca Fm., solid line: extrapolated curve, hollow circles: new points to be fitted by an exponential curve in b). b) Porosity versus depth graph including an exponential function that fits the new points for the Petaca Fm displayed in a). See the stratigraphic position of the Petaca Fm. in Fig. 3.

**Table 3**  
Initial porosity ( $\phi_0$ ) and compaction coefficient ( $c$ ) estimated for the different stratigraphic units using the methodology described in the text.

Unit	$\phi_0$	$c$
Chaco Fm. (Cenozoic)	0.38	0.331
Yecua Fm. (Cenozoic)	0.38	0.331
Petaca Fm. (Cenozoic)	0.38	0.331
Yantata Fm. (Cretaceous)	0.40	0.299
Ichoa Fm. (Cretaceous-Jurassic)	0.39	0.259
Carboniferous	0.36	0.371
Llmoncito Fm. (Devonian)	0.36	0.371
Roboré Fm. (Devonian)	0.39	0.383
Boomerang Fm. (Devonian)	0.36	0.371
Kirusillas Fm. (Silurian)	0.36	0.371

freehand drawn function (hollow circles in Fig. 12a) were plotted on a porosity versus depth graph and fitted by an exponential best-fit function (Fig. 12b). When no well data were available for a particular stratigraphic unit, well values obtained for lithologies comparable to this particular stratigraphic unit were employed. The initial porosity and the compaction coefficient for each stratigraphic unit derived from the method described above are displayed in Table 3.

6.3. Selection of the cross section location and orientation

The selected cross section runs across the most characteristic

structures and stratigraphic features of the studied area from the southern part, where Andean structures dominate, to the northern part, where pre-Andean structures are the main ones, and intersects or passes near a number of wells (Fig. 2). Since the orientation of the geological cross-section cannot be both parallel to the NE-SW average direction of the tectonic transport vector (so that the section is retrodeformable) and perpendicular to the E-W to ESE-WNW average strike of the structures (so that the section illustrates their proper geometry), the plane selected to build the cross section is vertical and its strike is N030E. The cross section was constructed by projecting the geological interpretations of the closest seismic profiles onto the selected cross-section plane, because none of the seismic profiles has the orientation of the chosen geological section.

6.4. Cross section description

The main structures in the central part of the cross section (Fig. 13) are: 1) two gentle to open detachment folds related to motion above the basal detachment located close to the base of the Kirusillas Fm. (Silurian), just above the basement top; and 2) a tectonic wedge including a possible shear-fault bend fold related to a backthrust which emanates from the basal detachment tip where the Paleozoic succession no farther north occurs. The most relevant structures in the northeast portion of the cross section (Fig. 13) are steep normal faults that cut and offset the uppermost part of the basement, the Mesozoic units and the lowermost Cenozoic unit (Petaca Fm.). These faults may have been active during the deposition of the Ichoa Fm. (Jurassic-Cretaceous) and the Petaca Fm. (Cenozoic), given that these stratigraphic units are thicker in their fault hangingwalls.

In addition to the variation of the structural style from southwest to northeast, there is also an important stratigraphic change (Fig. 13). The base of the Mesozoic rocks is an erosional unconformity, so that Mesozoic units lay directly on top of the pre-Silurian basement to the northeast, where Silurian-Devonian and Carboniferous rocks are absent, whereas they are deposited above progressively younger Paleozoic rocks to the southwest from the Kirusillas Fm. (Silurian) in the central part of the cross section to the Carboniferous in the southwest part of the section (Fig. 4). Furthermore, the Paleozoic sequence exhibits a wedge shape, so that it is thicker and more complete to the southwest.

6.5. Sequential restoration and decompaction of the cross section

The depth-converted 2D geological transect across the study area (Fig. 13), was sequentially restored to show the evolution of this portion of the study area. The restorations were performed using the geometric/kinematic algorithms called “flexural-slip” and “fault-propagation fold” implemented in the software Move©, and using a mechanical methodology based on the finite element method (FEM) applied to linear elastic deformation implemented in the software Dynel© (Maerten and Maerten, 2001). These 2D restoration algorithms were

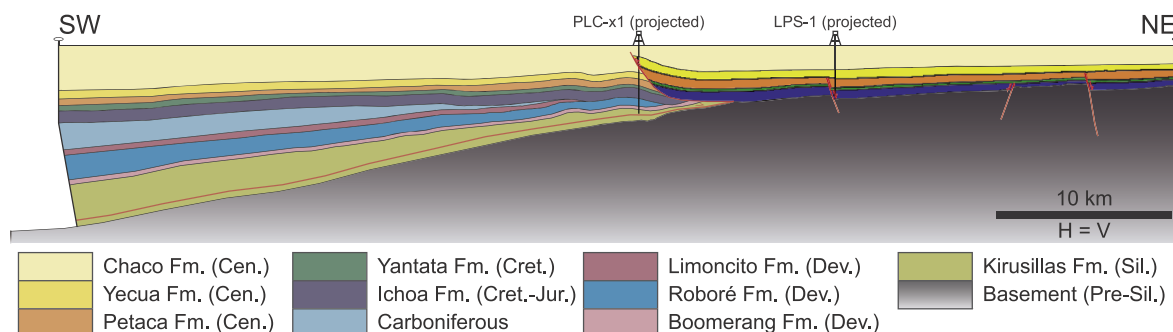


**Fig. 13.** Geological cross-section constructed by projecting the geological interpretations of nearby seismic profiles onto a N030E vertical plane. PLC: Palacios well drilling the Palacios anticline and LPS: Los Penocos well. See location in Fig. 2.

**Table 4**

Mean “true” (i.e. normal to the stratigraphic unit top) thickness in meters of the different stratigraphic units nowadays (0) and after each decompaction step (1–9).

Unit	0	1	2	3	4	5	6	7	8	9
Chaco Fm.	2463	–	–	–	–	–	–	–	–	–
Yecua Fm.	554	757	–	–	–	–	–	–	–	–
Petaca Fm.	416	520	590	–	–	–	–	–	–	–
Yantata Fm.	320	387	434	476	–	–	–	–	–	–
Ichoa Fm.	511	574	667	668	721	–	–	–	–	–
Carboniferous	1023	1131	1191	1230	1306	1475	–	–	–	–
Limoncito Fm.	547	578	598	617	644	743	976	–	–	–
Roboré Fm.	887	951	980	1004	1032	1112	1202	1332	–	–
Boomerang Fm.	336	353	362	370	381	410	429	461	648	–
Kirusillas Fm.	1255	1315	1340	1359	1381	1429	1478	1535	1695	1794

used because they are the ones that best emulate the particle motion caused by the most important structures in the geological cross-section. The pin line was placed at the northeast end of the geological cross-section and the loose line at the southwest edge. To show the thickness variations over time of the stratigraphic units, they were decompacted during the restoration using the software Move© and employing the functions obtained by ourselves for each stratigraphic unit (Table 4).

The first restoration step consisted of removing the displacement along the detachment and the backthrust and unfolding both the shear fault-bend fold and the detachment folds in the central part of the cross section; these must be the youngest structures since they involve Upper Cenozoic rocks (Fig. 14a). The mechanical restoration of these structures shows that strain was especially intense at the backlimb of the shear-fault bend fold and in the backthrust footwall close to the point where it merges with the basal detachment (Fig. 14b). The absolute value of the maximum strain achieved is 0.50. The strain computed in the mechanical restoration is the deformation suffered by the linear triangular elements in which the geological cross-section has been discretized in order to build a mesh (Maerten, 2010). The shortening values measured as the length of the restored section minus the length of the present-day, deformed section range from 1.5 km, in the case of the geometric/kinematic restoration, to 1.0 km, in the case of the mechanical restoration. Different values of shortening are obtained because all the shortening is consumed in displacement of the rocks to form thrusts and folds in the geometric/kinematic restoration, whereas part of the shortening is consumed in displacement to form thrusts and folds, and the remaining shortening is accommodated as strain suffered by the rocks in the mechanical restoration. The numerical results obtained from the restorations are not totally accurate due to possible errors made during the geological interpretation of the seismic data, the projection of the geological interpretations onto the chosen plane, the depth-conversion, the estimation of the decompaction functions and the angle of 17° between the section line and the average direction of the contractional tectonic transport vector. After returning the Cenozoic units to its initial horizontal position, these stratigraphic units were removed and the underlying succession was decompacted accordingly.

The displacement along the normal faults located in the northeast part of the cross section was removed in the next restoration step. This was performed in two stages, as they seem to have been active during two different times: during the deposition of the Petaca Fm. (lower Cenozoic) and during the sedimentation of the Ichoa Fm. (Jurassic-lower Cretaceous) (Fig. 14a). According to the mechanical restoration, the strain is mainly concentrated in the fault hangingwalls close to the faults, being 0.16 the maximum absolute value (Fig. 14b). The extension values measured as the length of the restored section minus the length of the section restored to a younger stage are negligible in both the geometric/kinematic and the mechanical restorations given that they are less than 0.1 km. Again, possible errors made during the geological interpretation of the seismic data, the projection of the geological interpretations onto the chosen plane, the depth-conversion, the estimation of the decompaction functions and the 30° angle

between the section line and the suspected direction of the extensional tectonic transport vector, make the quantitative results derived from the restorations approximate. As in the previous step, after each restoration the corresponding stratigraphic units were removed and the underlying units were decompacted.

Once all the folds and faults were restored, the main unconformity, located at the base of the Mesozoic rocks, was rotated to a horizontal disposition. After this, the Paleozoic units were sequentially restored to a horizontal attitude (Fig. 14a), which allowed illustrating the progressive tilting of the basement top in the southwest part of the study area as the deposition of the Silurian, Devonian and Carboniferous took place (Fig. 15). The basement top dip varied through time from around 3° to the SW in Ordovician times to about 11° nowadays. According to the mechanical restoration, the maximum strain took place in the hinge zone of the gentle flexure that involves the basement top and reached a maximum value of 0.60 (Fig. 14b). These dip and strain values are approximate due to the reasons explained above. Since some portions of the Paleozoic units below the pre-Mesozoic unconformity were eroded, they were reconstructed before their decompaction to obtain a more realistic result. The sequential restoration of the Paleozoic rocks allowed the detection of subtle sedimentary geometries similar to progressive unconformities that, otherwise, could have been neglected. For instance, the Boomerang and the Limoncito fms. (Devonian) are approximately tabular, whereas Kirusillas and Roboré fms. (Silurian and Devonian respectively) are wedge-shaped (Fig. 13). This thickness variation pattern may reflect subsidence changes, i.e. periods of relative quiescence would result in constant thicknesses and almost no rotation of the basement top, whereas accelerated subsidence might favor thickening towards the basin depocenter and rotation of the basement top (Fig. 15).

Thus, according to the restorations carried out, the maximum horizontal displacement values took place as shortening during the Late Cenozoic compressive episode (Andean), whereas the extension values during the Early Cenozoic and the Mesozoic extensional episodes (pre-Andean) were inferior. In the same way, the maximum strain values occurred during the Andean episode and during the basement tilting occurred in Paleozoic times.

## 7. Construction and restoration of a 3D model

### 7.1. 3D model generation

The geological interpretation of faults carried out on the seismic profiles and on the 3D seismic volumes was interpolated to create fault surfaces using the module called convergent interpolation implemented in the software Petrel©. Once the fault framework was built, the procedure was replicated with each of the tops of the stratigraphic units and unconformities, taking into account how these surfaces were cut and offset by the fault surfaces previously generated (Fig. 16). The resulting surfaces were depth-converted using the interval velocity model presented above to allow the correct visualization of their geometry, to

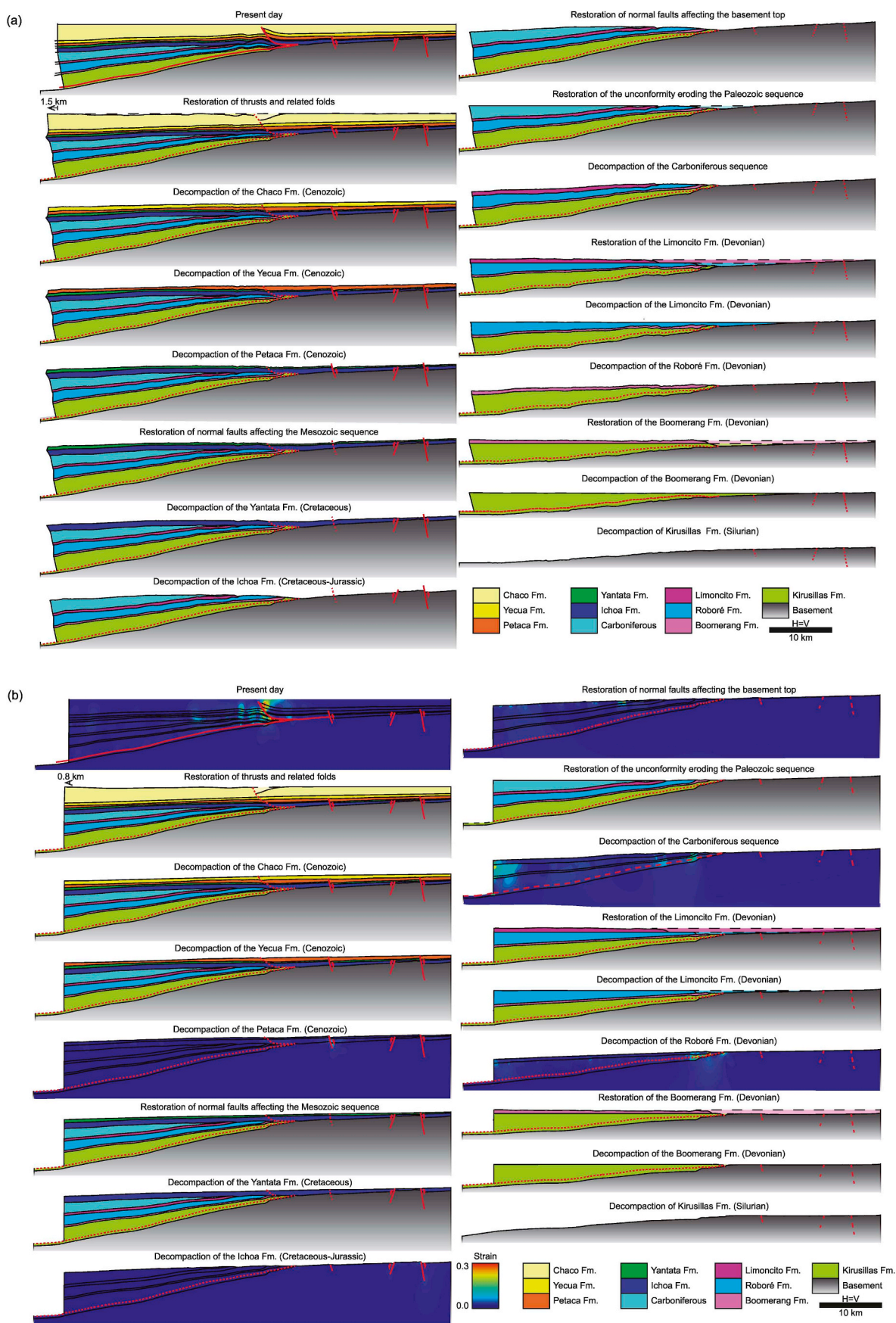
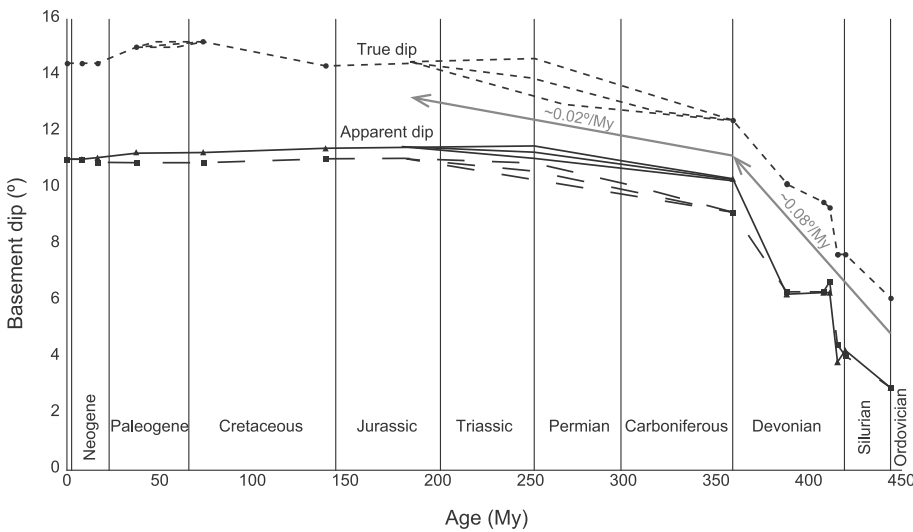
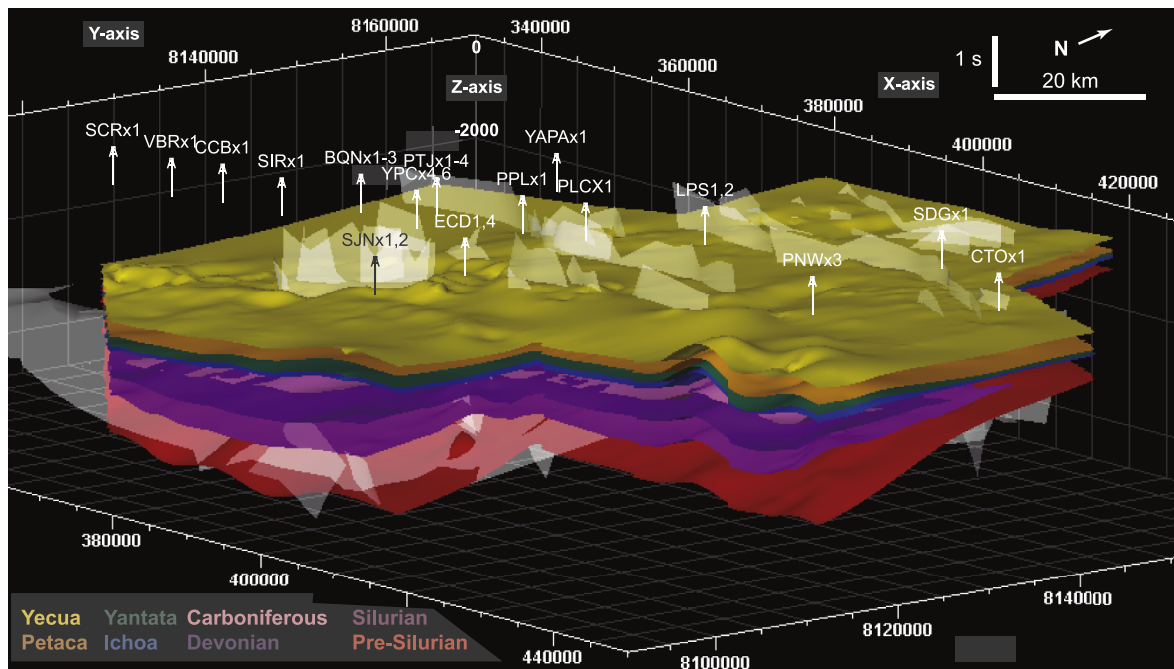


Fig. 14. 2D sequential restoration and decompaction of the geological cross-section shown in Fig. 13 using: a) the software Move© combining the flexural-slip and fault-propagation fold algorithms, and b) the software Dynel© using a finite element method (FEM) applied to linear elastic deformation. The dashed boundaries of the Carboniferous, Limoncito Fm. and Roboré Fm. in the north part of the restorations indicate that we ignore whether these stratigraphic units were or not deposited in this region.



**Fig. 15.** Evolution through time of the mean dip of the basement top in the south part of the study area derived from the sequential restoration of the geological cross-section illustrated in Fig. 14 (black solid line and black triangles: geometric/kinematic restoration, black dashed line and black squares: mechanical restoration), and from the sequential restoration of the 3D model illustrated in Fig. 17 (black dotted line and black circles: kinematic restoration). The grey arrows correspond to average tilting paths followed by the basement top with their corresponding rotation rates.



**Fig. 16.** 3D geological model of the study area showing the main faults and stratigraphic tops, as well as wells. Some tops, such as those corresponding to intra Devonian units, have not been shown in the model for the sake of clarity. Faults are displayed in white. The names of the wells are listed in Fig. 2 caption.

be able to measure dips and strikes, and to calculate burial depth and unit thicknesses. Finally, both the fault and stratigraphic surfaces were smoothed to avoid drawbacks during the restoration.

**7.2. Sequential restoration and decompaction of the 3D model**

Similarly to the cross section restoration, the depth-converted 3D model, i.e. the present-day, deformed 3D model (Fig. 16), was sequentially restored employing a geometric and geometric/kinematic algorithm called “flexural-slip” implemented in the software Move©. This 3D restoration algorithm was selected because it adequately simulates the activity of the main structures represented in the 3D geological model. Different pin and unfolding planes/surfaces were used for each of the main restoration steps. To restore the Cenozoic structures (first restoration stage), i.e. unfolding the cover folds related to motion along the basal detachment, the unfolding plane has the same orientation than the plane of the restored 2D cross-section, which is 120/90. The pin plane (030/90) is perpendicular to the unfolding plane

and is located to the north of the study area where almost no structures occur. Given that the second restoration stage consisted mainly of un-tilting progressively the basement top by removing the Silurian, Devonian and Carboniferous, wedge-shaped units (Fig. 17), the pin surface chosen is vertical and follows the hinge of the basement flexure (i.e. the transition from S-dipping to sub-horizontal basement top). The unfolding plane chosen (060/90) bisects the main bend of the hinge trace of the basement flexure in the central part of the study area (Fig. 2). The normal faults that offset part of the Cenozoic and Mesozoic sequences were not considered in this restoration given their small displacements. Moreover, the stratigraphic units were decompacted after each restoration step using the software Move© and the functions estimated above to determine their thickness (both vertical and normal to the top) at each time interval (Table 4).

The variation of the basement top dip in the south part of the study area was plotted on the graph in Fig. 15 to illustrate how this dip increased as the Paleozoic units were deposited. The average dip of the basement top varied from around 6° to the SW in Ordovician times to

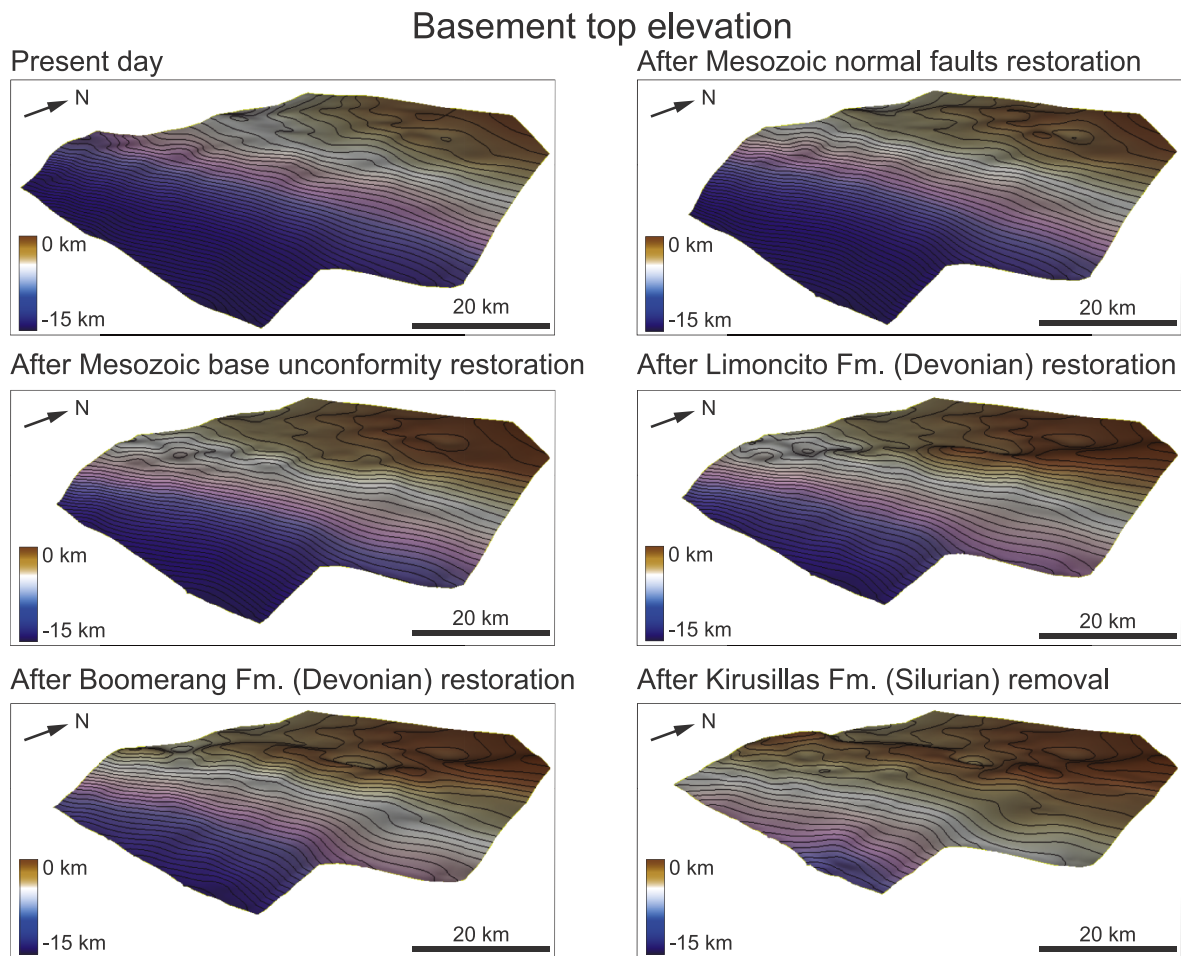


**Fig. 17.** 3D sequential restoration of the basement top surface extracted from the 3D model depicted in Fig. 16, carried out using the flexural-slip algorithm implemented in the software Move©. Contours each 250 m and vertical exaggeration x2.

about  $14^\circ$  nowadays. These values, derived from the 3D restoration, are slightly higher than those obtained from the 2D restoration. The reason is that the restored geological cross-section is oblique to the line of maximum dip of the basement top, and therefore, it shows apparent dips, whereas the dips extracted from the 3D geological model are true dips. Despite being true dips, these values may not be totally correct due to possible errors made during the geological interpretation of the seismic data, the construction of the 3D geological model, the depth-conversion, the estimation of the decompaction functions and the choice of the pin and unfolding planes/surfaces.

The graph in Fig. 15 shows various stages with notably different rates. The basement top dip would have increased at an average rate of approximately  $0.08^\circ/\text{My}$  during Silurian and Devonian, whereas it would have increased at a slower average rate of around  $0.02^\circ/\text{My}$  during Carboniferous and, probably, Permian and Triassic. The higher rotation rate of the basement top during Silurian and Devonian is interpreted as a result of rapid basin subsidence, while the lower rotation rate during Carboniferous and, probably, Permian and Triassic suggests slower basin subsidence. We are not sure about the subsidence causes, but the sedimentary load may have been one of them, given that the average sedimentation rate was  $48 \text{ m/My}$  during Silurian and Devonian, while it was  $25 \text{ m/My}$  during Carboniferous according to the decompacted thickness in Table 4. Another hypothesis to explain the rotation rate variations might be a widespread sedimentation during Carboniferous and Permian, which, in turn, would produce a generalized subsidence of the area, less focused on the south where the basement top dips to the S. On the contrary, the Devonian and Silurian sedimentation would have been concentrated in the south part of the

study area (as shown by the Silurian onlaps to the north) generating a heavier sedimentary load in the southern region.

The basement top dip is slightly higher during the Paleogene than during the Mesozoic and is slightly lower during the Neogene. The dip increase during Early Cenozoic might be interpreted as a result of lithosphere bending due to the load exerted by the weight of the sediments and Andean thrust sheets. The dip decrease during Late Cenozoic might result from the load reduction due to the exhumation triggered by the erosion of the relief created during the Andean orogeny.

### 7.3. Variation of unit thickness and burial depth through time

Table 4 shows the variation of the mean thickness for each stratigraphic unit as the overlying units were removed and the remaining units were decompacted using the decompaction functions estimated above. Two thickness values were computed: vertical thickness and true thickness (normal to the stratigraphic unit top). Only the true thickness variation is presented since the differences between the true and the vertical thickness are almost negligible, which is consistent with the fact that most of the horizons are sub-horizontal or display gentle dips. The thickness reduction suffered by the stratigraphic units from their deposition to nowadays is notable since it ranges from 30 to 50% (Table 5). Maps to illustrate the thickness of each stratigraphic unit throughout the study area at different times have been constructed by combining the 3D restoration together with the decompaction suffered by the units as the overlying units were removed. As an example, the thickness variation of the Roboré Fm. is depicted in Fig. 18. The maps show that the thickness variation was more significant in the central

**Table 5**  
Mean accumulated thickness change (%) after deposition of each stratigraphic unit from the Kirusillas Fm. of Silurian age (9) to the Chaco Fm. of Cenozoic age (0).

Unit	0	1	2	3	4	5	6	7	8	9
Chaco Fm.	0	-	-	-	-	-	-	-	-	-
Yecua Fm.	-27	0	-	-	-	-	-	-	-	-
Petaca Fm.	-29	-12	0	-	-	-	-	-	-	-
Yantata Fm.	-33	-19	-9	0	-	-	-	-	-	-
Ichoa Fm.	-29	-20	-7	-7	0	-	-	-	-	-
Carboniferous	-31	-23	-19	-17	-11	0	-	-	-	-
Limoncito Fm.	-44	-41	-39	-37	-34	-24	0	-	-	-
Roboré Fm.	-33	-29	-26	-25	-23	-17	-10	0	-	-
Boomerang Fm.	-48	-46	-44	-43	-41	-37	-34	-29	0	-
Kirusillas Fm.	-30	-27	-25	-24	-23	-20	-18	-14	-6	0

and southern parts of the study area where the initial thickness of this formation was greater. Since thickness variation due to decompaction is related to porosity lost, these maps can help to estimate the amount of porosity lost of a source or reservoir rock in different areas at each time interval.

Employing the restorations and considering the decompaction, we also constructed maps of burial depth over time for the tops of the different stratigraphic units, i.e. the vertical distance from one particular stratigraphic horizon to the paleotopographic surface. Only the burial depth maps corresponding to the Boomerang Fm. top are shown as an example (Fig. 19). The maps illustrate how the wedge shape of the Silurian, Devonian and Carboniferous rocks caused a depth increment more important to the south, and how the regular distribution of the Mesozoic and Cenozoic mega-sequences produced a diffuse increase in the burial depth. These maps, combined with additional information such as paleogeothermal gradient and so on, are useful tools to assess

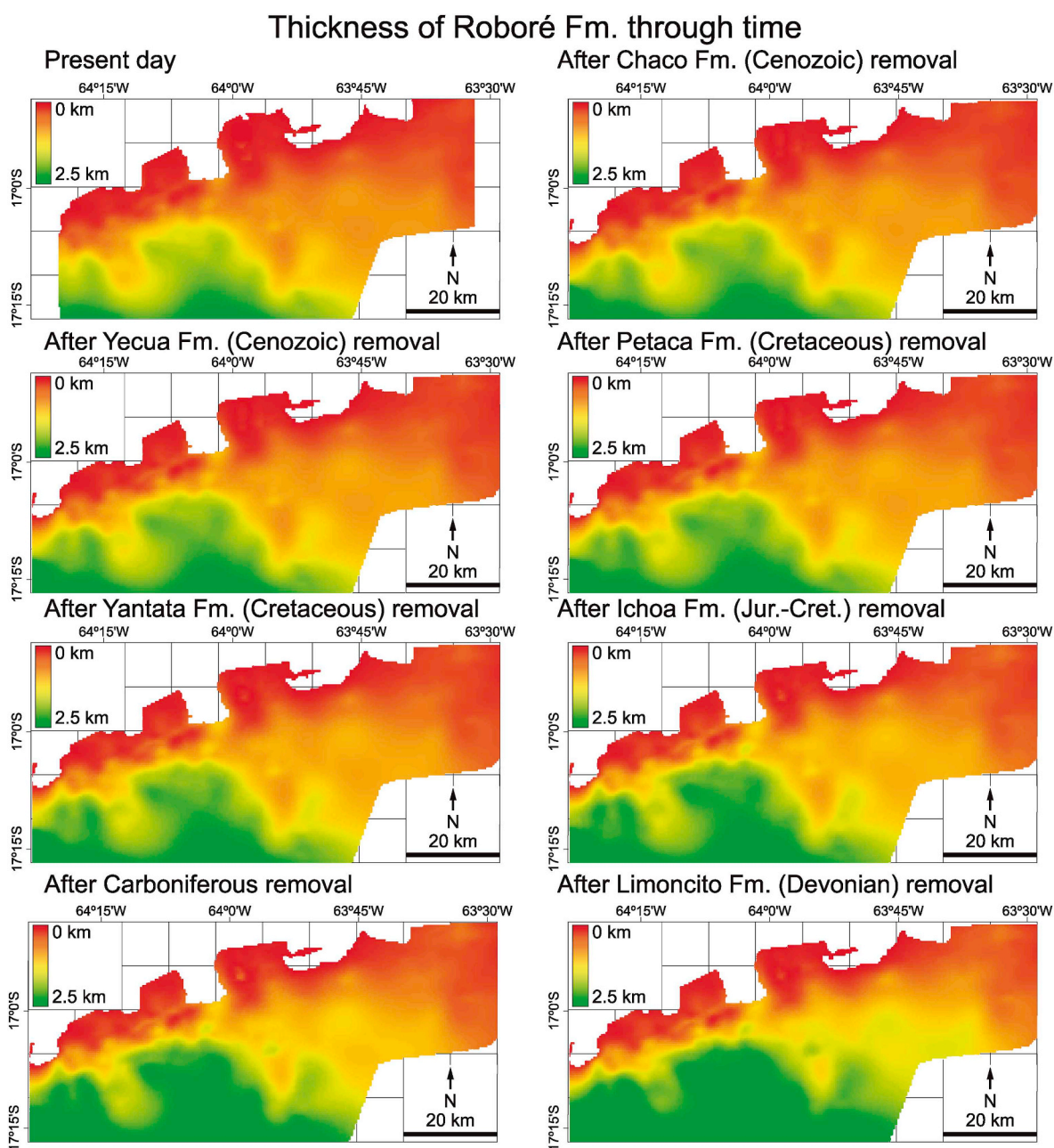


**Fig. 18.** Variation through time of the thickness of the Roboré Fm. of Devonian age (reservoir rock) in the study area (see location of the study area in Fig. 1). See the stratigraphic position of the Roboré Fm. in Fig. 3.



## Burial depth of Boomerang Fm. through time

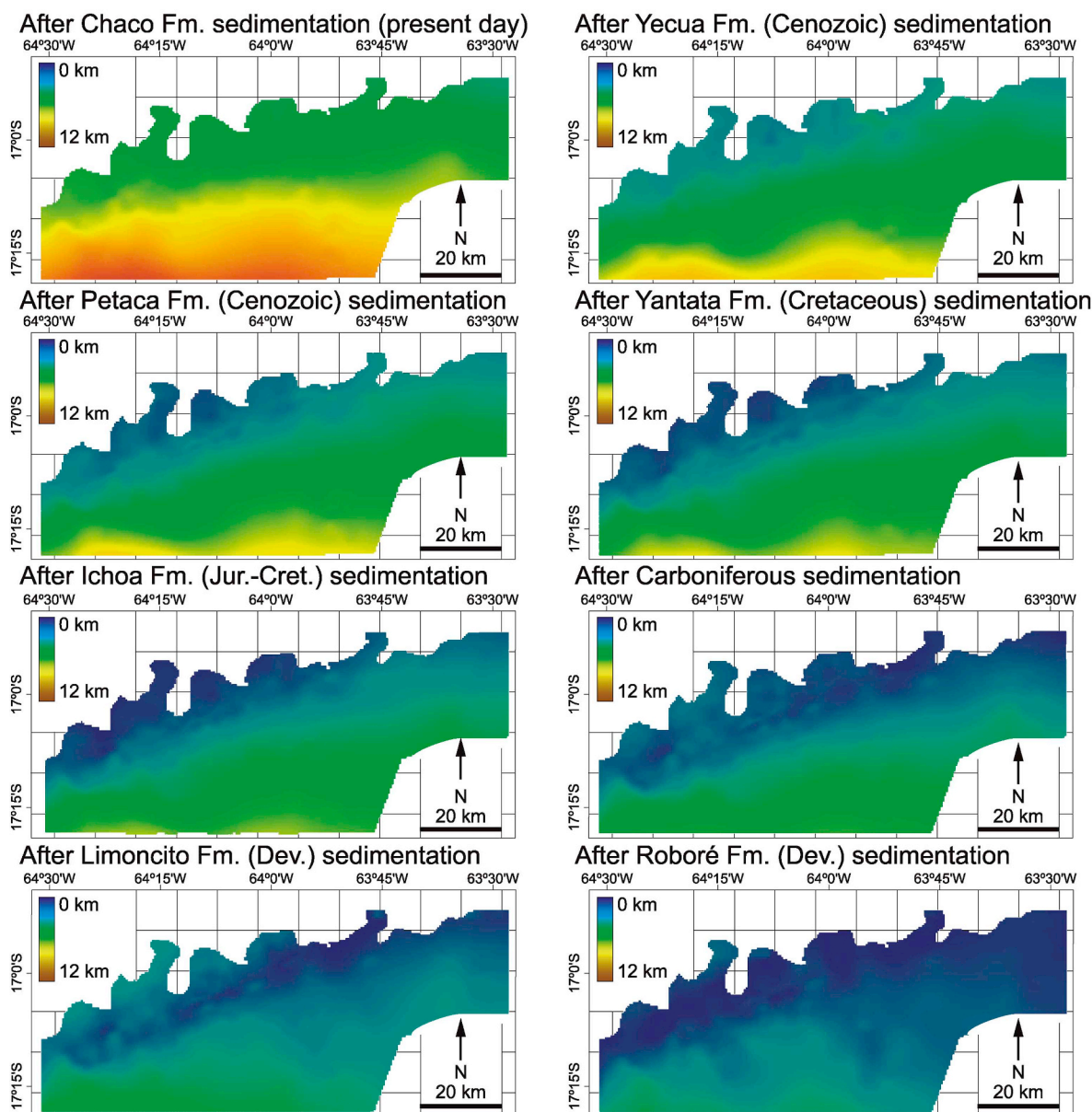


Fig. 19. Variation through time of the burial depth for the Boomerang Fm. top of Devonian age (source rock) in the study area (see location of the study area in Fig. 1). See the stratigraphic position of the Boomerang Fm. in Fig. 3.

which areas of the source rocks could enter the hydrocarbon maturation window at each time stage.

### 8. Controls on the Andean structure

The basal detachment runs along the shales located in the lower part of the Silurian succession, i.e. it took advantage of favorable ductile rocks. It terminates where these rocks are absent or they are very thin (Figs. 6–8). Thus, the location of the Andean basal detachment within the stratigraphic succession was mainly controlled by the mechanical stratigraphy of the Paleozoic succession (Baby et al., 1994; Welsink et al., 1995a; Kley, 1996; Anderson et al., 2017).

The present-day geometry of the basement top, sub-horizontal to the north and S-dipping in the southern region, would be the result of combining a paleorelief inherited from the Brazilian Shield (Hinsch et al., 2002) with progressive lithosphere flexure due to sedimentary, and perhaps tectonic, load. The wedge shape of the Silurian, Devonian

and Carboniferous rocks, and the onlap of the Silurian and Devonian on the basement top where it dips to the south (Figs. 3 and 6–8 and 13 and 16), point out that the basement top acquired its S dip during the Paleozoic, as shown in the restorations (Figs. 14 and 17) and in the graph in Fig. 15. Therefore, the region where the basement top dips to the S was the edge of a high in the Silurian-Carboniferous basin. In addition, this edge behaved as an extensional detachment during Paleozoic times and was reactivated as a contractional detachment during the Cenozoic (Fig. 6). Thus, the location, geometry, size and orientation of the frontal termination of the Andes (Figs. 2 and 5) was basically controlled by the edge of the Silurian-Carboniferous high (Hinsch et al., 2002), the extensional detachment and, probably the thinning towards the north of the Paleozoic sequence (Giraud and Limachi, 2001).

Tectonic wedges formed at the tip of the basal detachment where the Silurian and Devonian rocks onlap abruptly on the basement top, whereas faults and folds formed where they onlap smoothly on the basement top (Figs. 6–8). The tectonic wedge backthrust emanates from

the basal detachment tip when the ductile rocks lay only above the S-dipping portion of the basement top, whereas the backthrust emanates from an upper detachment connected to the basal detachment through a ramp when the ductile rocks lay above the S-dipping and above the sub-horizontal portions of the basement top. Thus, the type of Andean frontal structures was controlled by the geometry and position of the Silurian-Carboniferous rocks (Welsink et al., 1995a).

Although new Andean structures occur in the study area, various contractional structures formed in Cenozoic times resulted from mild, selective inversion tectonics of extensional structures inherited from Mesozoic and/or Paleozoic times, either in the form of reverse reactivation or thrusts that cut and offset previous extensional faults (Fig. 10). This situation is common in the Andean Cordillera, and it has been documented both at small and large-scale in the area (Sempere et al., 1991; Welsink et al., 1995a, 1995b; Mescua and Giambiagi, 2012; Perez et al., 2016). Thus, not only the Andean basal detachment and its associated frontal structures undergo control by pre-Andean structures, but other Andean-age structures are also influenced by previous structures.

The arguments above indicate that the location, morphology, dimensions and orientation of the frontal part of the Andes in the study area depended strongly on the basement configuration as well as on the Paleozoic stratigraphy. Therefore, the main orientation of the structures in the Boomerang Hills would not respond to a change in the tectonic transport direction, but to the control imposed by previous elements.

## 9. Tectono-stratigraphic evolution

After Precambrian times, an extensional regime evidenced by faults, occurred synchronously to Cambrian and Ordovician marine sedimentation (Fig. 20). In Ordovician times, a more uniform and widespread sedimentation took place which ended with a notable, regional angular unconformity during the Late Ordovician due to the Oclöyic orogeny (Tankard et al., 1995). This situation was replaced by a more widespread marine sedimentation in late Silurian to Devonian times, interpreted as the result of a relaxation in the extensional stresses (Bally and Snelson, 1980). The unconformity in the south part of the Boomerang Hills rotated, possibly due to subsidence, while in the north part remained approximately stable. The tilted region became the southern slope of a high, so that marine Silurian and Devonian sediments overlapped on it and thickened towards the basin depocenter located to the south. Above the high, Silurian rocks filled in small, depressed regions bounded by faults probably initiated during Silurian times. The contrast between rapid tilting rates during Silurian and Devonian times, and slower ones during Carboniferous, and maybe Permian-Triassic, caused a slight angular unconformity at the base of the continental Carboniferous rocks. Once the edge of the high was relatively steep, i.e. after sedimentation of Silurian-Devonian and before sedimentation of Jurassic, an extensional detachment, probably due to gravity, developed along the southern slope of the high (Fig. 20).

A noticeable erosion occurred between Carboniferous and Jurassic times, possibly resulting from basin uplift, gave place to a marked angular unconformity (see also Tankard et al., 1995) (Fig. 20). Thus, part of the Precambrian-Ordovician, Silurian, Devonian and Carboniferous rocks were eroded as well as any Permian and Triassic successions that had deposited in the region. This process could be related to a re-organization of the stresses in the area during Triassic times (Sempere, 1995). Uplift due to the rifting associated with the Atlantic Ocean opening in Mesozoic times (Nürnberg and Müller, 1991; Hall et al., 2018) is one of the hypotheses proposed to explain the erosion. Continental to shallow marine Jurassic and Cretaceous rocks sedimented unconformably over the underlying Precambrian-Paleozoic succession irrespective of whether this succession was tilted or untilted. Mesozoic was a tectonic quiescence period, although new normal faults developed during Jurassic-Early Cretaceous (Fig. 20). Part of the sedimentation was controlled by synsedimentary faults, although a

decrease in the extension intensity and a sea level rise would result in a less constrained subsidence (Sempere, 1994, 1995).

The basin emerged between Cretaceous and Cenozoic times, and the depositional environment change caused a paraconformity on which lower Cenozoic continental rocks sedimented throughout the entire area over Mesozoic rocks (Fig. 20). The dip in the southern part of the Boomerang Hills increased slightly during Early Cenozoic and synchronously a few normal faults developed in the northern part, some of them resulting from reactivation of old Mesozoic normal faults (see also Welsink et al., 1995a). The dip variation might result from lithosphere bending because of the sedimentary and tectonic loads caused by the weight of the Andean syn-contractional sediments and thrust sheets emplaced in more internal parts of the Cordillera, whereas the normal faults would have formed in the outer arc of the flexure. During late Cenozoic times a thick continental sequence deposited under relatively calm tectonic conditions. The subsequent Andean event, which would have started around Oligocene-late Miocene in the Central Andes (e.g. Sempere et al., 1990; Uba et al., 2006) and had propagated to the Subandean area about 10–12.5 Ma (e.g. Gubbels et al., 1993; Moretti et al., 1996; Uba et al., 2009; Lease et al., 2016), consisted of oblique reverse reactivation of the gravity-driven, extensional detachment of Paleozoic age, which became the Andean basal detachment, as well as development of folds and thrusts (Fig. 20). The Andean basal detachment became the Andean frontal thrust when propagated up to the hinge of the flexure that separates the southern slope of the Paleozoic basin high from the northern, elevated area. Thus, the Andean contractional structures affected mainly the Silurian-Devonian, Carboniferous, Mesozoic and Cenozoic rocks located above the southern slope of the Paleozoic basin high, although a few new thrusts and selective reactivation of some old normal faults as reverse faults occurred further north of the Andean frontal thrust in the portion of the Beni-Chaco Plain adjacent to the Andes. A slight dip decrease in the southern part of the Boomerang Hills occurred during Late Cenozoic. As in most mountain ranges, sedimentation, development of tectonic structures and denudation of the growing relief would have taken place simultaneously during this period. The dip decrease might be due to the fact that the balance between sedimentary/tectonic load with respect to denudation was favorable to the latter.

## 10. Hydrocarbon potential

The main source rocks for hydrocarbons in the study area are of Silurian, Devonian and, less important, Carboniferous age (Fig. 3). Reservoirs have been identified in the Silurian, Devonian (mainly Roboré Fm.), Mesozoic (Yantata and Ichoa fms.) and Cenozoic units (Yecua and Petaca fms.). Silurian, Devonian, Carboniferous and Cenozoic shales act as seals (e.g. Illich et al., 1981; Baby et al., 1995; Welsink et al., 1995a; Lindquist, 1998).

Those wells whose available information includes their geographical coordinates and hydrocarbon contents have been plotted on the structural map of the study area depicted in Fig. 2. The purpose of this map is trying to understand some relationships between the underlying geological structures and the wells position and hydrocarbon contents.

Most wells are located in the southern domain of the Boomerang Hills, i.e. in the Andes front, close to the basal detachment tip where: 1) the stratigraphic succession is quite complete and, as a consequence, source, reservoir and seal rocks are well developed (Fig. 3); and 2) there is a large number of structures, such as folds and thrusts, and therefore, large probabilities of structural traps (Figs. 2 and 5). Most of the successful wells are aligned following crests of anticlines along strike, which run approximately parallel to the trace of the basal detachment tip line, i.e. from E-W to ENE-WSW, and involve the cover mega-sequences, i.e. Silurian-Devonian, Carboniferous, Mesozoic and Cenozoic (Figs. 2, 6, 7, 9 and 13). In contrast, unsuccessful wells are usually located away from the crest of the anticlines. There are fewer wells in

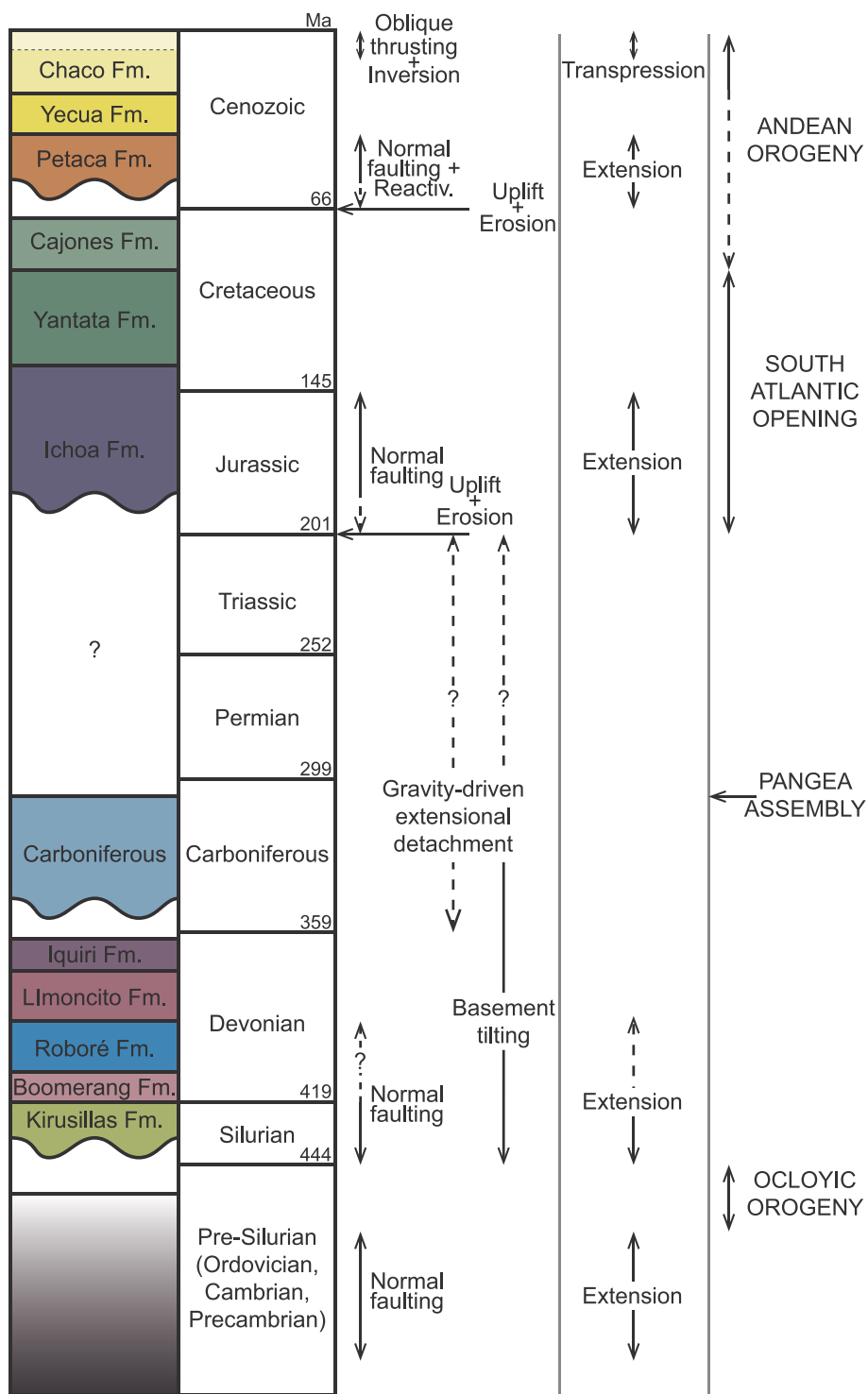


Fig. 20. Stratigraphic column of the Boomerang Hills including the large-scale tectonic events, the tectonic regimes, and the structures formed during each event. Wavy lines: erosive unconformities, dashed lines: unconformities without evidence of erosion. Stratigraphic and time columns on the left modified from Baby et al. (1995) and Welsink et al. (1995a). Geodynamic setting column on the right modified from Tankard et al. (1995).

the northern domain of the Boomerang Hills, i.e. in the Beni-Chaco Plain, where: 1) the stratigraphic succession is more incomplete because Paleozoic source rocks are almost missing, except for Silurian shales preserved in sporadic depressions (Fig. 3); and 2) the density of tectonic structures, and therefore, of possible structural traps, is lower than in the southern domain (Figs. 2 and 5). Most of the wells are located along the eastern portion of an ESE-WNW to E-W striking, N-dipping, long normal fault which offsets the pre-Silurian basement, as

well as the Mesozoic and the lower part of the Cenozoic cover mega-sequences (Fig. 2). These wells drill the fault hangingwall near the fault surface (Figs. 6 and 13). The central and western parts of this fault have not yet been explored. Other wells located, presumably, at the crest of anticlines related to inverted or reverse faults have not found hydrocarbon shows.

Oil discoveries are more frequent in the wells drilled in the northern domain of the Boomerang Hills, whereas gas is more common in the

southern domain wells (Fig. 2 and Table 1). Moreover, in the northern domain all the productive wells contain a certain amount of oil, whereas in the southern domain there are wells that contain only gas. Thus, the spatial distribution of gas and oil might be conditioned to a certain extent by the age of the Andean structures; the oldest structures would contain both, while the youngest ones may contain gas solely. From a subsurface study and its comparison with laboratory physical experiments, Baby et al. (1994) concluded that the hydrocarbon migration in this region ended in the time interval between the development of the Andean contractional structures located in the outer part of the southern domain and that of the innermost ones, that is, in Late Cenozoic. The fact that hydrocarbons are found in the hangingwall of normal faults developed during Early Cenozoic suggests that, if only a single hydrocarbon migration stage took place, it began by the Early Cenozoic and ended in the Late Cenozoic.

## 11. Conclusions

Two domains have been identified from the tectono-stratigraphic point of view in the Boomerang Hills. In the southern domain, which is the buried frontal part of the Andean Cordillera, the structural style corresponds mostly to thin-skinned contractional tectonics, the structures are mainly Andean (Late Cenozoic) folds and faults, and the stratigraphic succession is thick and almost complete including five mega-sequences separated by unconformities: a Precambrian-Ordovician basement and four cover mega-sequences of Silurian-Devonian, Carboniferous, Mesozoic and Cenozoic age. In the northern domain, which belongs to the portion of the Beni-Chaco Plain adjacent to the Andes, the structural style is mostly thick-skinned of extensional type, the structures are mainly pre-Andean (Cambrian to Early Cenozoic) faults, and the stratigraphic sequence is thinner because Silurian-Carboniferous rocks are almost missing.

The three most striking structural events occurred in the Boomerang Hills are: 1) formation of growth normal faults during three Pre-Andean extensional events of Cambrian-Ordovician, Silurian, and Jurassic-Early Cretaceous age, and normal reactivation of previous faults during early Cenozoic (Andean); 2) flexure of the south part of the basement due to quick subsidence during the Silurian-Devonian and slower during the Carboniferous and possibly Permian-Triassic, so that the dipping portion of the basement became the southern slope of a high and behave as a gravity-driven, extensional detachment; and 3) reactivation of the extensional detachment as the basal detachment of oblique thrusts and folds developed during a transpressional event of late Cenozoic age (Andean), as well as selective reactivation of inherited normal faults. The largest amount of displacement took place in the form of shortening during the Andean event, while the maximum strain values were achieved during the Andean event and during the basement rotation of Paleozoic age.

The Paleozoic configuration of this region exerted a strong influence on the main features of the frontal part of the Andes in terms of types of structures, and their orientation, position and size. Thus, the position of the Andean basal detachment within the ductile Silurian rocks was controlled by the mechanical stratigraphy of the Paleozoic succession, and its orientation, geometry and dimensions replicated the orientation, shape and size of a pre-Andean extensional detachment/slope of a basin high. The development of one or another type of frontal structure (tectonic wedge or faults and folds) responded to the angular relationships, geometry and location of the Paleozoic cover rocks and the underlying basement.

The workflow followed in this study, which incorporates geological interpretation of 2D/3D seismic data and wells, construction of a transect across the area by projecting adjacent geological interpretations, construction of a 3D model, geometric/kinematic and mechanical restoration in 2D and 3D accompanied by decompaction, and construction of maps over time of different stratigraphic units derived from the present-day 2D sections, from the 3D model restorations and from

the decompaction, has proven to be a valuable tool in order to characterize the main structures, as well as decipher the structural history of the Boomerang Hills. The results obtained may be a first step to better understand the hydrocarbon distribution in this province, and therefore, to improve the exploitation of discovered hydrocarbon fields and to make new findings.

## CRedit authorship contribution statement

**Hodei Uzkeda:** Conceptualization, Methodology, Formal analysis, Data curation, Writing - original draft, Visualization. **Mayte Bulnes:** Conceptualization, Formal analysis, Writing - review & editing, Visualization, Funding acquisition. **Josep Poblet:** Conceptualization, Writing - original draft, Visualization, Project administration, Funding acquisition. **Gonzalo Zamora:** Conceptualization, Resources, Writing - review & editing, Funding acquisition.

## Acknowledgements

H. Uzkeda has been supported by research contract CN-16-014 (“Convenio específico para la realización de un trabajo de investigación post-doctoral en la disciplina de Geología”) under the framework agreement between Repsol Exploración S.A. and the University of Oviedo. We are grateful to Repsol Exploración S.A. for providing the well and seismic data. We thank J. Flinch, M. Masini and B. Amigo from Repsol Exploración S.A. for helping us with the data and contracts. We would like to acknowledge financial support by research project CGL 2015-66997-R (“Aplicación del análisis del plegamiento a la investigación de recursos geológicos” -AAPLIREGE-) funded by the Spanish Ministry for Economy and Competitiveness and the European Fund for Regional Development (FEDER), and research project FC-GRUPIN-IDI/2018/000216 (“Ayudas a organismos públicos de investigación para apoyar la actividad que desarrollen sus grupos de investigación en el Principado de Asturias en el periodo 2018–2020”) funded by the Principado de Asturias. We thank Midland Valley and Petroleum Exploration Experts for permission to use the software Move© (Academic site software license and support agreement number 1915/Contract reference Agr\_ULA\_UniOviedo\_18\_11\_01), Schlumberger for permission to use the software Petrel© and Dynel© (Academic agreement 1-1C5GCE1 Revision 1), HIS Markit for permission to use the software Kingdom Suite© (University Grant Program), and Richard Allmendinger and Nestor Cardozo for permission to use the software Stereonet. We also thank J.G. Antuña for maintaining the software for seismic interpretation, restoration and modeling. Comments by the Editor Bernard Colletta, as well as Patrice Baby and anonymous reviewers have substantially improved the final version of the manuscript.

## Appendix A. Supplementary data

Supplementary data to this article can be found online at <https://doi.org/10.1016/j.marpetgeo.2020.104299>.

## References

- Anderson, R.B., Long, S.P., Horton, B.K., Calle, A.Z., Ramirez, V., 2017. Shortening and structural architecture of the Andean foldthrust belt of southern Bolivia (21°S): implications for kinematic development and crustal thickening of the central Andes. *Geosphere* 13 (2), 538–558.
- Angevine, C.L., Heller, P.L., Paola, C., 1990. Quantitative sedimentary basin modelling. *AAPG Contin. Educ. Course Note Ser.* 32, 1–161.
- Baby, P., Herail, G., López, J.M., Oller, J., Pareja, J., Sempere, T., Tufiño, D., 1989. Structure de la Zone subandine de Bolivie: influence de la géométrie des séries sédimentaires antéorogéniques sur la propagation des chevauchements. *Comptes Rendus de l'Académie des Sciences. Série 2* 309 (17), 1717–1722.
- Baby, P., Moretti, I., Guillier, B., Limachi, R., Mendez, E., Oller, J., Specht, M., 1995. Petroleum systems of the northern and central Bolivian sub-Andean zone. In: Tankard, A.J., Suárez S, R., Welsink, H.J. (Eds.), *Petroleum Basins of South America*. vol. 62. AAPG Memoir, pp. 445–458.

- Baby, P., Specht, M., Oller, J., Montemurro, G., Colletta, B., Letouzey, J., 1994. The Boomerang-Chaparé transfer zone: structural interpretation and experimental approach. In: Roure, F., Ellouz, N., Shein, V.S., Skvortsov, I. (Eds.), *Geodynamic Evolution of Sedimentary Basins*, International Symposium, Moscow, Russia, pp. 203–218.
- Bally, A.W., Snelson, S., 1980. Realms of subsidence. In: Miall, A.D. (Ed.), *Facts and Principles of World Petroleum Occurrence*, vol. 6. Canadian Society of Petroleum Geologists Memoir, pp. 9–94.
- Bevis, M., Kendrick, E., Smalley JR, R., Brooks, B., Allmendinger, R., Isacks, B., 2001. On the strength of interpolate coupling and the rate of back arc convergence in the central Andes: an analysis of the interseismic velocity field. *G-cubed 2* (2001GC000198), 1–16.
- Bond, G.C., Kominz, M.A., Devlin, W.J., 1983. Thermal subsidence and eustasy in the Lower Paleozoic miogeocline of western North America. *Nature* 306, 775–779.
- Carey, S.W., 1958. The orocline concept in geotectonics. *Proc. Royal Soc. Tasmania* 89, 255–258.
- Dunn, J.F., Hartshorn, K.G., Hartshorn, P.W., 1995. Structural styles and hydrocarbon potential of the sub-Andean thrust belt of southern Bolivia. In: Tankard, A.J., Suárez S, R., Welsink, H.J. (Eds.), *Petroleum Basins of South America*, vol. 62. AAPG Memoir, pp. 523–543.
- Geobolivia, 2000. Mapa Geológico de Bolivia. escala 1:1 000 000.
- Giraud, R., Limachi, R., 2001. Pre-Silurian control in the genesis of the central and southern Bolivian fold belt. *J. S. Am. Earth Sci.* 14 (7), 665–680.
- Gubbels, T.L., Isacks, B.L., Farrar, E., 1993. High-level surfaces, plateau uplift, and foreland development, Bolivian Central Andes. *Geology* 21, 695–698.
- Hall, S.A., Bird, D.E., Mclean, D.J., Towle, P.J., Grant, J.V., Danque, H.A., 2018. New constraints on the age of the opening of the South Atlantic basin. *Mar. Petrol. Geol.* 95, 50–66.
- Hindle, D., Kley, J., Klosko, E., Stein, S., Dixon, T., Norabuena, E., 2002. Consistency of geologic and geodetic displacements during Andean orogenesis. *Geophys. Res. Lett.* 29 (8) 29–31 – 29–34.
- Hinsch, R., Krawczyk, C.M., Gaedicke, C., Giraud, R., Demuro, D., 2002. Basement control on oblique thrust sheet evolution: seismic imaging of the active deformation front of the Central Andes in Bolivia. *Tectonophysics* 355, 23–39.
- Hinsch, R., Krawczyk, C.M., Andina-Boomerang Team, Giraud, R., Demuro, D., Rebay, G., Goitia, V.H., 2003. Structural modelling and deformation balancing in the foothills of the Bolivian Andes: constraints on accretion kinematics in curved thrust belts. *Revista Técnica de YPF* 21, 117–124.
- Husson, L., Moretti, I., 2002. Thermal regime of fold and thrust belts—an application to the Bolivian sub Andean zone. *Tectonophysics* 345, 253–280.
- Illich, H.A., Haney, F.R., Mendoza, M., 1981. Geochemistry of oil from Santa Cruz basin, Bolivia: case study of migration-fractionation. *AAPG (Am. Assoc. Pet. Geol.) Bull.* 65 (11), 2388–2402.
- Isacks, B.L., 1988. Uplift of the central Andean plateau and bending of the Bolivian orocline. *J. Geophys. Res.: Solid Earth* 93 (B4), 3211–3231.
- Kley, J., 1996. Transition from basement-involved to thin-skinned thrusting in the Cordillera Oriental of southern Bolivia. *Tectonics* 15 (4), 763–775.
- Kley, J., 1999. Geologic and geometric constraints on a kinematic model of the Bolivian orocline. *J. S. Am. Earth Sci.* 12, 221–235.
- Klosko, E.R., Stein, S., Hindle, D., Kley, J., Norabuena, E., Dixon, T., Liu, M., 2002. Comparison of GPS; seismological, and geological observations of Andean mountain building. *Plate Bound. Zones* 30, 123–133.
- Laffite, G., Del Vo, S., Aguilera, E., Goitia, V., Rebay, G., Lanussol, D., 1998. The Petroleum Systems of the Boomerang Area. AAPG Search and Discovery, Bolivia Article #90933.
- Lease, R.O., Ehler, T.A., Enkelmann, E., 2016. Large along-strike variations in the onset of Subandean exhumation: implications for Central Andean orogenic growth. *Earth Planet Sci. Lett.* 451, 62–76.
- Lindquist, S.J., 1998. The Santa Cruz – Tarija Province of Central South America: Los Monos – Machareti (I) Petroleum System. US Geological Survey Open-File Report, pp. 16 99-50-C.
- Maerten, F., 2010. Geomechanics to Solve Geological Structure Issues: Forward, Inverse and Restoration Modeling. PhD thesis. Université Montpellier II, pp. 455.
- Maerten, F., Maerten, L., 2001. Dynel: a new 3-D geomechanical method for modeling geological structures. *Stanford Rock Fract. Proj.* 12, E1–E10.
- Mercier, J.L., Sebrrier, M., Lavenu, A., Cabrera, J., Bellier, O., Dumont, J.-F., Machare, J., 1992. Changes in the tectonic regime above a subduction zone of Andean type: the Andes of Peru and Bolivia during the Pliocene-Pleistocene. *J. Geophys. Res.* 97 (B8), 11945–11982.
- Mescua, J.F., Giambiagi, L.B., 2012. Fault inversion vs. new thrust generation: a case study in the Malargüe fold-and-thrust belt, Andes of Argentina. *J. Struct. Geol.* 35, 51–63.
- Mingram, A., Russo, A., Pozzo, A., Cazau, L., 1979. Sierra Subandinas. In: *Proceedings of the Segundo Simposio Geología Regional Argentino*, Córdoba, Argentina, pp. 95–138.
- Moretti, I., Baby, P., Méndez, E., Zubieta, D., 1996. Hydrocarbon generation in relation to thrusting in the Subandean zone from 18° to 22°S, south Bolivia. *Petrol. Geosci.* 2, 17–28.
- Moretti, I., Labaume, P., Sheppard, S.M.F., Boulègue, J., 2002. Compartmentalisation of fluid migration pathways in the sub-Andean Zone, Bolivia. *Tectonophysics* 348, 5–24.
- Nürnberg, D., Müller, R.D., 1991. The tectonic evolution of the south Atlantic from late jurassic to present. *Tectonophysics* 191 (1–2), 27–53.
- Perez, N.D., Horton, B.K., Carlotto, V., 2016. Structural inheritance and selective re-activation in the central Andes: Cenozoic deformation guided by pre-Andean structures in southern Peru. *Tectonophysics* 671, 264–280.
- Sempere, T., 1994. Kimmeridgian? to Paleocene tectonic evolution of Bolivia. In: Salfity, J.A. (Ed.), *Cretaceous Tectonics in the Andes: Earth Evolution Sciences Monograph Series*. Vieweg Publications, Wiesbaden, pp. 168–212.
- Sempere, T., 1995. Phanerozoic evolution of Bolivia and adjacent regions. In: Tankard, A.J., Suárez S, R., Welsink, H.J. (Eds.), *Petroleum Basins of South America*, vol. 62. AAPG Memoir, pp. 207–230.
- Sempere, T., Baby, P., Oller, J., Hérail, G., 1991. La napa de Calazaya: una prueba de acortamientos importantes controlados por elementos paleoestructurales en los Andes bolivianos. *Revista Técnica de YPF* 12, 229–234.
- Sempere, T., Hérail, G., Oller, J., Bonhomme, M.G., 1990. Late Oligocene-Early Miocene major tectonic crisis and related basins in Bolivia. *Geology* 18, 946–949.
- Suppe, J., Connors, C.D., Zhang, Y., 2004. Shear fault-bend folding. In: McClay, K.R. (Ed.), *Thrust Tectonics and Hydrocarbon Systems*, vol. 82. AAPG Memoir, pp. 303–323.
- Tankard, A.J., Uliana, M.A., Welsink, H.J., Ramos, V.A., Turic, M., França, A.B., Milani, E.J., De Brito Neves, B.B., Eyles, N., Skarmeta, J., Santa Ana, H., Wiens, F., Cirbián, M., López Paulsen, O., Germs, G.J.B., De Wit, M.J., Machacha, T., Miller, R.M.C.G., 1995. Structural and tectonic controls of basin evolution in Southwestern Gondwana during the Phanerozoic. In: Tankard, A.J., Suárez S, R., Welsink, H.J. (Eds.), *Petroleum Basins of South America*, vol. 62. AAPG Memoir, pp. 5–52.
- Uba, C.E., Heubeck, C., Hulka, C., 2006. Evolution of the late Cenozoic Chaco foreland basin, southern Bolivia. *Basin Res.* 18, 145–170.
- Uba, C.E., Kley, J., Strecker, M.R., Schmitt, A.K., 2009. Unsteady evolution of the Bolivian Subandean thrust belt: the role of enhanced erosion and clastic wedge progradation. *Earth Planet Sci. Lett.* 281, 134–146.
- Welsink, H.J., Franco, M.A., Oviedo, G.C., 1995a. Andean and pre-Andean deformation, Boomerang Hills area, Bolivia. In: Tankard, A.J., Suárez S, R., Welsink, H.J. (Eds.), *Petroleum Basins of South America*, vol. 62. AAPG Memoir, pp. 481–499.
- Welsink, H.J., Martínez, E., Aranibar, O., Jarandilla, J., 1995b. Structural inversion of a Cretaceous rift basin, southern Altiplano, Bolivia. In: Tankard, A.J., Suárez S, R., Welsink, H.J. (Eds.), *Petroleum Basins of South America*, vol. 62. AAPG Memoir, pp. 305–324.